

RESEARCH

Open Access



Advancing colorectal cancer therapy with biosynthesized cobalt oxide nanoparticles: a study on their antioxidant, antibacterial, and anticancer efficacy

Fateme Momen Eslamiehei¹, Mansour Mashreghi^{1,2} and Maryam M. Matin^{1,3*}

*Correspondence:
matin@um.ac.ir

¹ Department of Biology, Faculty of Science, Ferdowsi University of Mashhad, Mashhad, Iran

² Industrial Biotechnology Research Group, Institute of Biotechnology, Ferdowsi University of Mashhad, Mashhad, Iran

³ Novel Diagnostics and Therapeutics Research Group, Institute of Biotechnology, Ferdowsi University of Mashhad, Mashhad, Iran

Abstract

Background: Colorectal cancer (CRC) ranks as the third most common cancer globally and the second leading cause of cancer-related mortality. Traditional chemotherapy, while effective, often results in significant side effects, highlighting the need for more efficient cancer therapies. Recent advancements in nanotechnology have led to the development of strategies that aim to minimize toxicity to normal cells by more precise targeting of cancer cells. In this context, cobalt oxide nanoparticles (Co₃O₄ NPs) have shown promising anticancer potential. Our study focuses on evaluating the antioxidant, antibacterial, and anticancer properties of Co₃O₄ NPs synthesized using *Vibrio* sp. VLC, a bioluminescent bacterium.

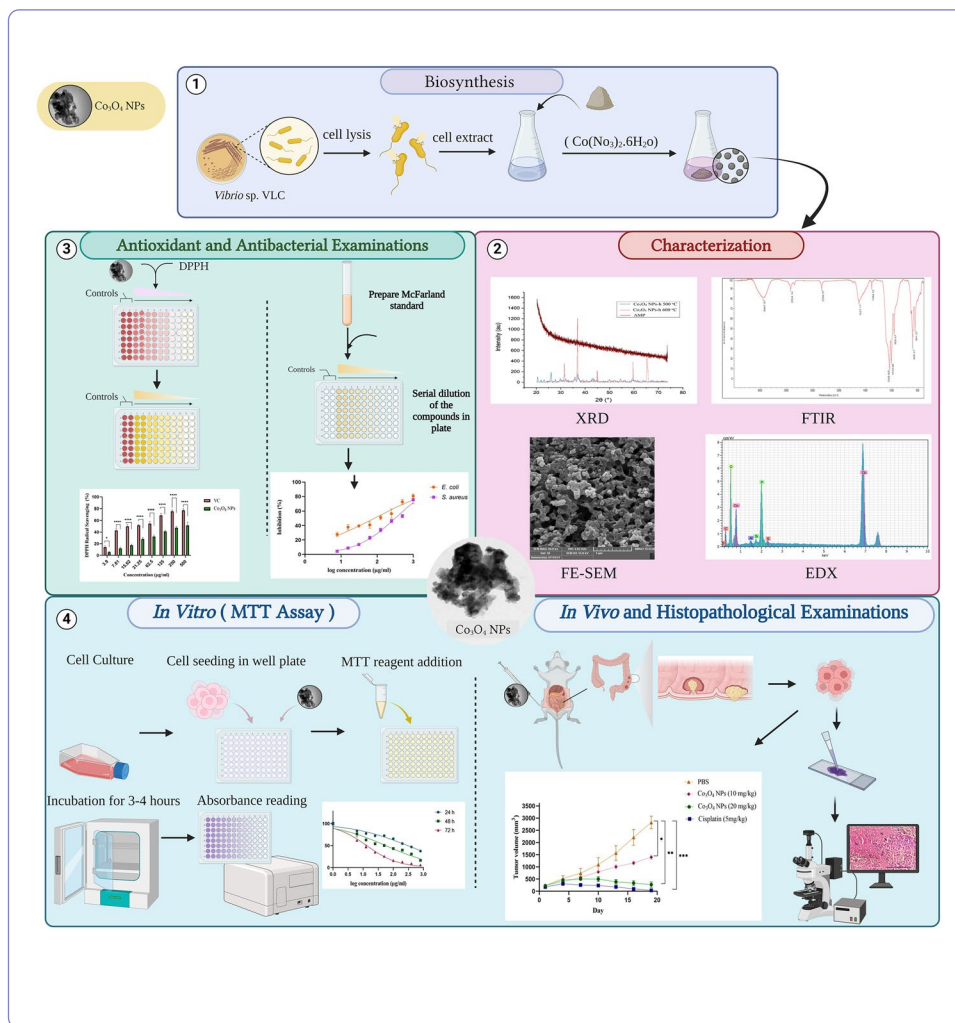
Results: XRD and FTIR analyses confirmed the successful synthesis of Co₃O₄ NPs, which displayed spherical morphology with an average diameter of 60 nm. The nanoparticles demonstrated significant antioxidant and antibacterial activities. The MTT assay indicated that the NPs caused dose- and time-dependent toxicity against CT26 cells, while exhibiting relatively lower toxicity towards normal cells. In vivo experiments further confirmed the significant tumor suppressive effects in BALB/c mice, with minimal side effects on the liver, spleen, and kidney tissues compared to the widespread toxicity of cisplatin.

Conclusion: This study verifies the successful synthesis of Co₃O₄ NPs and their potent antioxidant, antibacterial, and anticancer activities. The biosynthesized Co₃O₄ NPs represent a promising targeted method for CRC therapy. However, further research is needed to elucidate their mechanism of action and also their application in the clinical phase.

Keywords: Cobalt oxide nanoparticles (Co₃O₄ NPs), Biological synthesis, Colorectal cancer, Luminescent bacterium, CT26 cell line

Graphical Abstract





Background

Colorectal cancer (CRC) remains a significant global health challenge due to its high incidence and mortality rates. Despite advancements in the traditional treatment modalities, such as chemotherapy and radiation therapy, the quest for more effective and less toxic therapeutic options persists. In this context, nanotechnology emerges as a revolutionary approach, offering promising strategies for CRC treatment. Nanoparticles, due to their unique physicochemical properties, provide a versatile platform for cancer therapy, enabling targeted drug delivery, reduced systemic toxicity, and enhanced therapeutic efficacy. Nanoparticles can be engineered to selectively target cancer cells, facilitating the delivery of therapeutic agents and enabling image-guided treatments (Bhatia et al. 2022). Recent studies have highlighted the significant potential of nanoparticles in CRC treatment; for instance, the targeted delivery of chemotherapeutic agents using nanoparticles has been shown to increase drug accumulation in tumor cells, thereby enhancing antitumor activity while reducing the side effects (Huang et al. 2021). Additionally, nanoparticles have been employed as carriers for genes and RNA molecules, offering a novel method to gene therapy for CRC (Abrishami et al. 2024b; Lombardo et al. 2019).

The application of metal oxide nanoparticles, including Co_3O_4 NPs, has received considerable attention in cancer research due to their unique properties, such as magnetic responsiveness and photocatalytic activity, which can be exploited for therapeutic purposes (Iravani and Varma 2020). Cobalt salt exhibits strong cytotoxic effects on various cell types, but when transformed into cobalt oxide nanoparticles, it demonstrates selective toxicity towards cancer cells. These nanoparticles hold immense potential for diverse biological applications owing to their small size, large surface area, and high reactivity (Huang et al. 2021; Iravani and Varma 2020; Yu et al. 2022). A variety of methods, including physical, chemical, and biological approaches, have been employed to synthesize Co_3O_4 NPs. Recent advancements in synthesis techniques have expanded the potential applications of cobalt oxide nanoparticles, particularly in cancer therapy (Huang et al. 2021; Kalam et al. 2012). While there has been limited research on the utilization of biological materials such as bacteria, fungi, and plant extracts for the synthesis of cobalt oxide nanoparticles, it is essential to consider the desired size, shape, and surface chemistry of the nanoparticles when selecting the appropriate technique (Huang et al. 2021). Co_3O_4 NPs have shown great promise in cancer treatment due to their ability to induce oxidative stress in cancer cells, leading to cell death through apoptosis or necrosis (Shete et al. 2022). These nanoparticles have demonstrated high toxicity towards cancer cells while maintaining a reasonable level of safety for normal cells (Das and Saikia 2023). Furthermore, the incorporation of targeting ligands into Co_3O_4 NPs can enhance their selectivity towards cancerous cells (Lombardo et al. 2019). Additionally, Co_3O_4 NPs have been utilized in combination with chemotherapy drugs to enhance drug delivery and therapeutic efficacy (Huang et al. 2021).

The biosynthesis of nanoparticles presents an eco-friendly and cost-effective alternative to conventional synthesis methods, leveraging biological entities like bacteria, fungi, and plant extracts. This green synthesis method not only aligns with the principles of sustainability but also enhances the biocompatibility and therapeutic efficacy of nanoparticles (Das and Saikia 2023).

The use of bacteria in synthesizing nanoparticles, known as biological synthesis, offers several advantages. Firstly, bacteria play a crucial role in reducing metal ions, facilitating the synthesis process. Additionally, they act as capping agents, by controlling the size and shape of nanoparticles, which leads to the enhancement of their stability. Moreover, biological nanoparticles often exhibit excellent biocompatibility due to their organic coating, which make them suitable for biomedical applications. Their biological origin also contributes to their eco-friendliness. Overall, leveraging bacteria in nanoparticle synthesis not only improves efficiency but also enhances the biocompatibility and stability of the resulting nanoparticles (Huang et al. 2021; Iravani and Varma 2020; Jang et al. 2015).

Moreover, recent advancements in nanotechnology have underscored the significance of plant materials not only in the synthesis and stabilization of metallic nanoparticles but also in their application for cancer therapeutics. Plant extracts, rich in phytochemicals, offer a green and efficient method for the synthesis of nanoparticles, acting as both reducing and capping agents that confer stability and biocompatibility to the nanoparticles (Kavaz et al. 2018, 2019; Umar et al. 2023a, 2023b).

To date, there have been limited studies on the environmentally friendly synthesis of Co_3O_4 NPs using bacteria alone, with only a few reports available worldwide (Huang et al. 2021). Furthermore, no study has investigated the potential anticancer effects of biologically synthesized Co_3O_4 NPs on CT26 CRC cells in both in vitro and in vivo settings. In this study, Co_3O_4 NPs were biologically produced using *Vibrio* luminous bacteria. After characterizing their properties, the nanoparticles were assessed for their antioxidant and antibacterial activities as well as their cytotoxic effects on CT26 mouse CRC cells both in vitro and in vivo.

Methods

Bacteria and cell culture

Nanoparticles were synthesized using the luminescent bacterium *Vibrio* sp. VLC, which was cultured in sea water complex (SWC) medium for this study.

The CT26 cell line, derived from mouse colorectal cancer, and the NIH/3T3 cell line, derived from mouse embryonic fibroblasts, were obtained from Ferdowsi University of Mashhad (FUM). The CT26 cells were cultured in Roswell Park Memorial Institute (RPMI) 1640 medium supplemented with 10% fetal bovine serum (FBS), while the NIH/3T3 cells were cultured in Dulbecco's modified Eagle's medium–high glucose (DMEM-HG). Both cell lines were maintained in a humidified environment with 5% CO_2 at 37 °C. All experimental protocols involving the use of CT26 and NIH/3T3 cell lines were approved by the institutional review board and the ethics committee of FUM, under the approval number IR.UM.REC.1401.01.

Animals

Male BALB/c mice, aged 6 to 8 weeks, were bred and housed in the animal facility at the university. The animals were maintained in a climate-controlled environment with a 12 h light/dark cycle, a temperature of approximately 25 °C, and a humidity level of around 55%. The animal studies were approved by the ethics committee at FUM.

Synthesis of cobalt oxide nanoparticles

For the biological synthesis of cobalt oxide nanoparticles, a bacterial lysis solution of *Vibrio* sp. VLC was prepared. The bacteria were cultured in a liquid SWC medium and allowed to grow for 48 h. The resulting culture was centrifuged at 5000g for 15 min at 4 °C to separate the cells and eliminate the bacterial residues. The obtained sediment was washed with distilled water and subsequently homogenized in an additional 150 ml distilled water, and incubated at room temperature for 24 h. Subsequently, the suspension was centrifuged at 15 °C for 20 min to separate the supernatant, which was utilized for nanoparticle production. In this experiment, 100 ml bacterial cell lysis extract was mixed with 50 ml $\text{Co}(\text{NO}_3)_2 \cdot 6\text{H}_2\text{O}$ (a ratio of 2:1 and 0.15 mol/l), and the mixture was then incubated in a warm water bath for 90 min.

The suspension containing the purple precipitate was subjected to centrifugation at 16,500g for 10 min at 4 °C to initiate the separation and purification processes. In order to clean the sediment, it was washed with ethanol and distilled water. Subsequently, the

precipitate was subjected to overnight heating at 60 °C, followed by annealing at 500 and 600 °C for 2 h. These steps were conducted to enhance the purity and crystalline structure of the nanoparticles (Abdurakhmonov et al. 2022; Bechelany et al. 2010).

The yield of Co₃O₄ NPs production was calculated by weighing the final nanoparticles (after annealing at 600 °C for 2 h) obtained from a known volume of the reaction mixture (Eq. 1) (Riddin et al. 2006).

$$\text{Yield(\%)} = \left(\frac{\text{Mass of heated nanoparticles(g)}}{\text{Total mass of reactants used(g)}} \right) \times 100 \quad (1)$$

The exact concentration of nanoparticles in the stock solution, prepared for biological activity assays, was determined by dissolving a known mass of nanoparticles after annealing at 600 °C for 2 h in a defined volume of solvent (DMEM-HG culture medium), resulting in a stock solution with a concentration expressed in mg/ml. The concentration was calculated using the Eq. 2.

$$\text{Concentration(mg/ml)} = \frac{\text{Mass of nanoparticles(mg)}}{\text{Volume of solvent(ml)}} \quad (2)$$

Additionally, dynamic light scattering (DLS) and zeta potential analysis were utilized to investigate the size distribution and stability of the nanoparticles in suspension, further informing the effective concentration of nanoparticles in biological interactions (Kavitha et al. 2017; Cuello et al. 2020). The integration of these methodologies ensures a rigorous and reproducible method to nanoparticle synthesis, characterization, and application in biological systems. Through careful calculation of the yield and its concentration, this study may contribute valuable data to the field of nanomaterials research, offering insights into the scalability and biological efficacy of biosynthesized Co₃O₄ nanoparticles.

Characterization of the biosynthesized Co₃O₄ NPs

XRD and FTIR

The crystalline structure and the effect of annealing on decreasing the impurity rate of Co₃O₄ NPs were confirmed through high-resolution X-ray diffraction (XRD) and Fourier-transform infrared (FTIR) analysis. XRD was performed using a Cu K α radiation source operating at 40 kV and 40 mA. The analysis was conducted on powders of Co₃O₄ NPs, which were synthesized with a concentration of 0.15 mol/l, both before and after annealing at 500 and 600 °C. The crystal size was calculated using the Debye–Scherrer equation (Eq. 3).

$$D = \frac{K \cdot \lambda}{\beta \cdot \cos \theta} \quad (3)$$

In the Debye–Scherrer equation, D represents the crystallite size, λ is the wavelength of the X-ray radiation, K is a constant (commonly taken as 0.89), θ is the Bragg angle of the peak, and β is the full width at half maximum (FWHM) after subtracting instrumental broadening (Yang et al. 2010; Stanjek and Häusler 2004). Moreover, the biosynthetic mechanism of Co₃O₄ NPs was investigated using FTIR analysis to explore potential interactions between Co ions and biological molecules in both annealed and unheated

samples. In this study, the biosynthesis method was successfully examined by analyzing the powder of nanoparticles before and after annealing at 600 °C (Thermo Nicolet AVATAR 370 FTIR, USA).

FE-SEM, EDX, and elemental mapping

In order to examine the size, surface structure, elements, and the percentage of cobalt relative to oxygen, the nanoparticle powder synthesized with a concentration of 0.15 mol/l and annealed at 600 °C was analyzed using a field emission-scanning electron microscope (FE-SEM), energy-dispersive X-ray spectroscopy (EDX), and elemental mapping. In order to prepare the sample, the Co_3O_4 NPs powder was coated with a layer of gold, and then evaluated (FE-SEM ZEISS Sigma 300, Germany). The specific elemental compounds present in the sample and their relative abundance were identified using the EDX method. Additionally, elemental mapping was conducted on electron microscope images to determine the ratio of certain elements present in the samples (Scimeca et al. 2018).

TEM, HR-TEM, AFM, DLS, and zeta potential

The biosynthesized Co_3O_4 NPs were characterized for their size, shape, and morphology using transmission electron microscopy (TEM), high resolution- transmission electron microscopy (HR-TEM), atomic force microscopy (AFM), and DLS techniques. To prepare the samples, Co_3O_4 NPs powder was ultrasonicated in ethanol and then sprinkled over carbon-coated gold TEM grids and carbon-coated HR-TEM grids. The grids were allowed to dry prior to measurements. TEM imaging was conducted using an accelerating voltage of 100 kV (TEM Philips EM 208S, Netherlands), while HR-TEM imaging was performed at 200 kV (HR-TEM FEI TEC9G20, USA) (Chen et al. 2014). The AFM analysis was carried out on a stock solution of Co_3O_4 NPs that were annealed at 600 °C and dispersed in DMEM-HG + FBS (1:1 ratio) (Bibi et al. 2017). Furthermore, DLS was employed to determine the average size of nanoparticles after annealing at 600 °C in different media, including RPMI 1640, DMEM-HG, and distilled water. In order to prepare the sample, Co_3O_4 NPs powder was ultrasonicated in different media and then subjected to analysis (Cordouan 3 vasco, France) (Jang et al. 2015). The zeta potential of cobalt oxide nanoparticles at neutral pH in RPMI 1640 (+ FBS, ratio 1:1), DMEM-HG (+ FBS, 1:1 ratio), and distilled water was also investigated using the Zeta Compact Potential Analyzer device at the central laboratory of Ferdowsi University of Mashhad.

Preparation of cobalt oxide nanoparticle stock solutions

Co_3O_4 NPs were weighed and suspended in the DMEM-HG + FBS (1:1 ratio), at a concentration of 10 mg/ml. The suspension was stirred continuously overnight to achieve a thorough mixing, followed by sonication for 30 min to ensure a homogeneous dispersion of the nanoparticles. The resulting stock solution can be stored in a dark place at 4 °C until use.

Antioxidant activity

In this study, the antioxidant properties of the nanoparticles were evaluated using the 1,1-diphenyl-2-picrylhydrazyl (DPPH) free radical reduction method. DPPH is an unstable free radical that can be stabilized by accepting an electron (Brand-Williams et al. 1995; Zhu et al. 2011). The absorbance of the DPPH stock solution was measured at 517 nm. Methanol was added to the mixture until the absorbance value reached 0.98. As a positive control, vitamin C, a natural antioxidant, was used at concentrations ranging from 3.9 to 500 µg/ml. Co₃O₄ NPs were prepared at a concentration of 1000 µg/ml, and a series of dilutions were made in a 96-well plate. Following this step, 500 µl of the mixture of ethanol and DPPH was added to each well. The plate was then incubated in the dark at room temperature for 30 min. After that, the absorbance at 517 nm was measured using a spectrophotometer (Unico, Germany), and the data were collected with three repetitions for each concentration. The antioxidant activity of different concentrations of nanoparticles was compared to that of vitamin C using Eq. 4.

$$\text{DPPH radical scavenging activity (\%)} = \frac{(AC - AS)}{AC} \times 100 \quad (4)$$

In this equation, AC represents the absorption of the control, and AS represents the absorption of the sample (Ghadi et al. 2018).

Antibacterial activity

The antibacterial properties of the nanoparticles were assessed against both Gram-negative *Escherichia coli* (*E. coli*) and Gram-positive *Staphylococcus aureus* (*S. aureus*) bacteria.

Measuring the minimum growth inhibitory concentration (MIC)

To measure the minimum inhibitory concentration (MIC) of the nanoparticles, 100 µl Mueller Hinton Broth culture medium with a 2 × concentration was added to each well of the first column of a 96-well plate, while in the remaining wells, 100 µl Mueller Hinton Broth with 1 × concentration was added. 100 µl of the nanoparticles, in a stock suspension with the concentration of 2000 µg/ml, were added to the wells of the first column. A dilution series of the nanoparticles was then prepared in subsequent rows of the culture plate, extending up to the 10th row. Following the preparation of pure cultures of bacteria in Mueller Hinton broth, half of McFarland's standard for each bacterium was prepared. Subsequently, 10 µl of each bacterial suspension was added to the respective wells of the 96-well plate. The culture plates were then incubated at 37 °C and 150 rpm for a period of 24 h. The MIC₅₀ of the nanoparticles was calculated using Eq. 5, as described in previous studies (Iravani and Varma 2020; Gheidari et al. 2020; Durán et al. 2016; Hosseini-Giv et al. 2021).

$$\text{Inhibition (\%)} = 1 - \frac{a - (b + c)}{d - b} \quad (5)$$

In Eq. 5, the variables are defined as follows: a represents the absorbance of the wells containing different concentrations of substances with bacteria; b represents the

absorbance of the wells containing nutrient broth culture medium (negative control); c represents the absorbance of different concentrations of substances without bacteria (blank); and d represents the absorbance of wells containing medium with bacteria (positive control) (Arsalan et al. 2020). The data were collected with three repetitions for each concentration. The inhibition graph was generated using GraphPad Prism 8 software, and the concentration at which half of the bacterial growth was inhibited was determined as the MIC₅₀.

Cytotoxic studies

To assess the cytotoxic effects of Co₃O₄ NPs synthesized using *Vibrio* sp. VLC bacterial extract, both in vitro and in vivo experiments were conducted. In vitro cytotoxicity studies were performed using the MTT (3-[4,5-dimethylthiazole-2-yl]-2,5-diphenyltetrazolium bromide) assay, while tumor measurement and histopathological analyses were employed for in vivo evaluation.

MTT assay

The cytotoxic effects of the biosynthesized Co₃O₄ NPs were assessed against CT26 CRC cells as well as NIH/3T3 normal cell line. The cancer cells were cultured in RPMI 1640 medium containing 10% FBS, while the normal cells were cultured in DMEM-HG supplemented with 10% FBS. The CT26 and NIH/3T3 cells were seeded in 96-well plates at densities of 6×10^3 and 1×10^4 cells/well, respectively.

After incubating the cells for 24 h, they were treated with different concentrations of cisplatin (ranging from 3.125 to 100 µg/ml) and Co₃O₄ NPs (ranging from 6.25 to 800 µg/ml) for durations of 24, 48, and 72 h. Subsequently, the MTT assay was performed in the 96-well plates. The MTT solution, prepared at a concentration of 5 mg/ml in phosphate-buffered saline (PBS), was added to each well, and the plates were incubated for 3 h. The culture medium was then replaced with dimethyl sulfoxide (DMSO), and the samples were incubated for an additional 25 min. The formation of formazan crystals, indicative of viable cells, was detected using an ELISA reader at 545 nm wavelength (Stat Fax, USA) (Iranpour et al. 2021; Hosseini-Giv et al. 2021).

In vivo experiments

To induce colorectal tumors, a subcutaneous injection of 5×10^5 CT26 cells was administered into the right flank of male BALB/c mice (Sato et al. 2021; Gong et al. 2021). Once the tumor reached a volume of approximately 150 mm³, the animals were subjected to intraperitoneal injection of PBS (as a control), cisplatin (at a concentration of 5 mg/kg), and Co₃O₄ NPs (at concentrations of 10 and 20 mg/kg) once every three days for a total of 16 days (6 injections in total) (Chattopadhyay et al. 2014b, 2014a; Arghiani et al. 2014).

Measurement of tumor volume

The volume of CT26 tumors in BALB/c mice was measured from day 1 to day 19 following the injection of cisplatin and Co₃O₄ NPs. The tumor volumes were determined using Eq. 6, which involved measuring the length and width of the tumors using a caliper (Mitutoyo, Tokyo, Japan):

$$\text{Tumor volume} = \frac{A \times B^2}{2} \quad (6)$$

In this equation, A and B are the length (mm) and width (mm) of the tumor, respectively (Owyang et al. 2017; Chattopadhyay et al. 2014b; Hosseini-Giv et al. 2021).

Histopathological analysis

After the completion of the injection period, mice were euthanized using CO₂, and their organs, including liver, kidney, spleen, and tumor, were dissected and fixed in a 10% paraformaldehyde solution for histological analysis. The tissues were then processed, embedded in paraffin blocks, and sectioned into thin slices of approximately 4 μm thickness, followed by hematoxylin and eosin (H&E) staining (Sigma-Aldrich, Germany). The stained tissue sections were examined under a microscope at a magnification of 400× to observe histological features. Descriptions of the tumor type and pathological characteristics in all tissue samples were determined by a pathologist (Dr. Shaterzadeh, Mashhad, Iran). The extent of necrosis was assessed by investigating the necrotic areas in H&E-stained tumor sections, following previously established methods (Wang et al. 2021; Gong et al. 2021).

Results

Observable detection of Co₃O₄ NPs

The purity of the bacteria was assessed by observing their luminescence in the SWC culture medium and confirming the formation of single colonies (Fig. 1a, b). As shown in Fig. 1c–f, the color of the synthesis reaction solution changed from clear to purple, indicating the successful synthesis of nanoparticles. In the control group, which was exposed only to lysed extracts of bacteria, no color change was observed.

Characterization of Co₃O₄ nanoparticles

XRD and FTIR

The XRD and FTIR spectra of the Co₃O₄ NPs are shown in Fig. 2. The reflections in XRD spectra after heating are consistent with the spherical phase of Co₃O₄ NPs, as indicated by JCPDS No. 76–1802. The absence of peaks corresponding to impurity phases, demonstrates the high purity of the final products, which were calcined at 600 °C for 2 h (Fig. 2a). The peaks observed in the XRD spectrum at 2θ values of 31.92 (220), 37.46 (311), 44.72 (400), and 65.11 (404) are in accordance with the data provided by the International Center for Diffraction Analysis. The presence of protein molecules in the bacterial lysis biomass led to a shift in certain peaks, while other crystallographic contaminants may be attributed to the biomass sources. The average size of the nanoparticles was estimated to be approximately 18 nm using the Debye-Scherrer equation. Further, the biosynthesized Co₃O₄ NPs, both before and after annealing at 600 °C, were characterized using FTIR spectra in the wave number ranges of 400–4000 cm⁻¹. The spectra revealed the presence of various functional groups within the biosynthesized Co₃O₄ NPs obtained from the cellular extract of *Vibrio* sp. VLC bacteria. In Fig. 2b, sharp peaks at 3478 cm⁻¹, 2927 cm⁻¹, 1648–1530 cm⁻¹, and 1067–1227–1397 cm⁻¹ are indicative of hydroxyl groups, amino groups, amide I and II groups, and C–H₂ bonds,

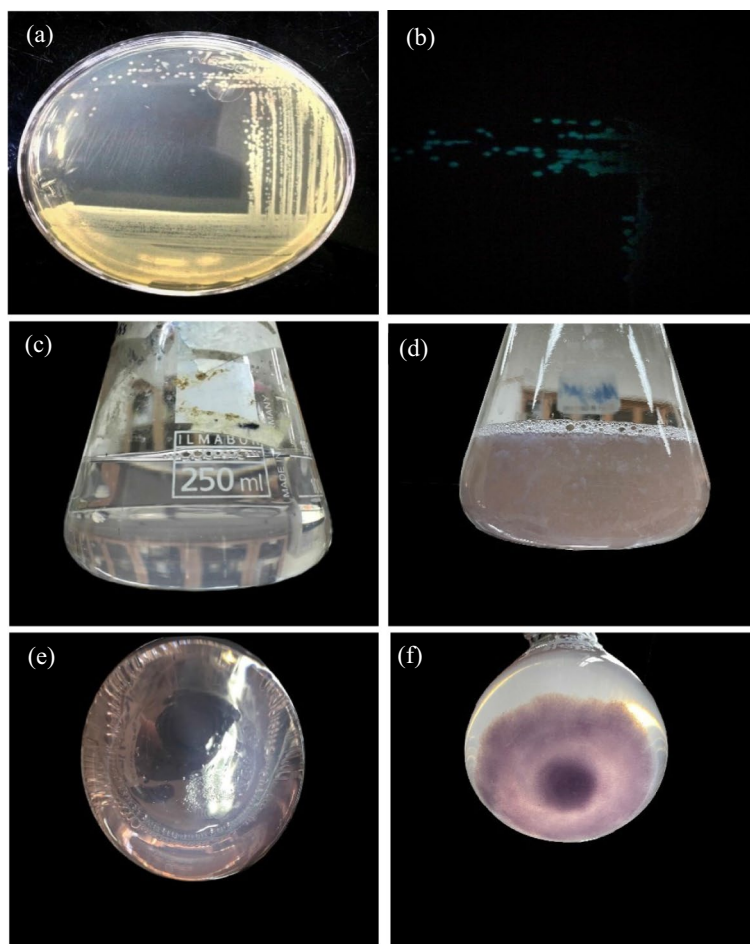


Fig. 1 *Vibrio* sp. VLC pure culture and visual observation of sediment formation of Co_3O_4 NPs. **a** Yellow colonies formed by *Vibrio* sp. VLC on SWC medium in the presence of light. **b** Yellow colonies formed by *Vibrio* sp. VLC in the absence of light. **c, e** Before mixing bacterial cell extract with $\text{Co}(\text{NO}_3)_2 \cdot 6\text{H}_2\text{O}$. **d** After 90 min of mixing bacterial cell extract with $\text{Co}(\text{NO}_3)_2 \cdot 6\text{H}_2\text{O}$ and incubation in a hot water bath. **f** 1 h after the end of synthesis. The cloudy and violet-color sediments in pictures (**d, f**) represent cobalt oxide nanoparticles

respectively. The effects of heating and annealing were observed to reduce the presence of biological impurities during the biosynthesis of Co_3O_4 NPs, as evidenced by a decrease in the intensity of functional group peaks and noise in the annealed sample. The formation of Co_3O_4 NPs is indicated by a peak at 567 cm^{-1} in Fig. 2b and peaks at 561 cm^{-1} and 605 cm^{-1} in Fig. 2c, which correspond to the characteristic vibrations of Co–O bonds.

FE-SEM, EDX, and elemental mapping

FE-SEM analysis was employed to examine the size and morphology of the biosynthesized Co_3O_4 NPs. Additionally, the EDX analysis was conducted on the Co_3O_4 NPs synthesized using *Vibrio* sp. VLC bacteria extract prior to the calcination process to assess the presence of biological compounds in the bacterial extract. According to FE-SEM micrographs, the Co_3O_4 NPs exhibited a spherical shape, with an average size of 65–67 nm (Fig. 3a–c). The EDX analysis confirmed the presence of cobalt and oxygen

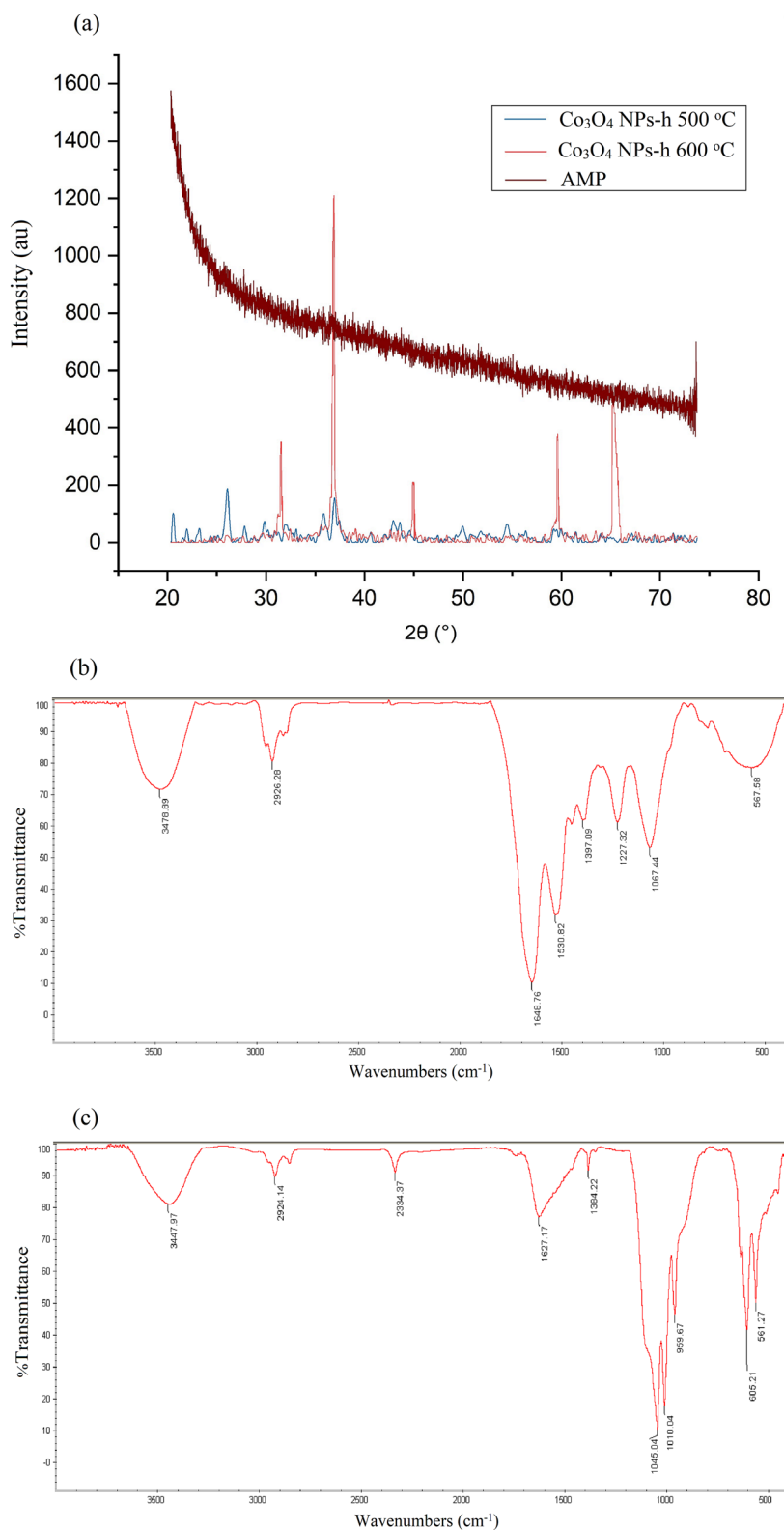


Fig. 2 X-ray diffraction (XRD) and Fourier-transform infrared (FTIR) spectra of Co_3O_4 NPs. **a** XRD spectrum of Co_3O_4 NPs before heating in the furnace (AMP), after heating at 500 $^\circ\text{C}$ for 2 h (Co_3O_4 NPs-h 500 $^\circ\text{C}$), and after heating at 600 $^\circ\text{C}$ for 2 h (Co_3O_4 NPs-h 600 $^\circ\text{C}$). **b** FTIR spectrum of Co_3O_4 NPs before annealing, and **c** after annealing at 600 $^\circ\text{C}$ for 2 h

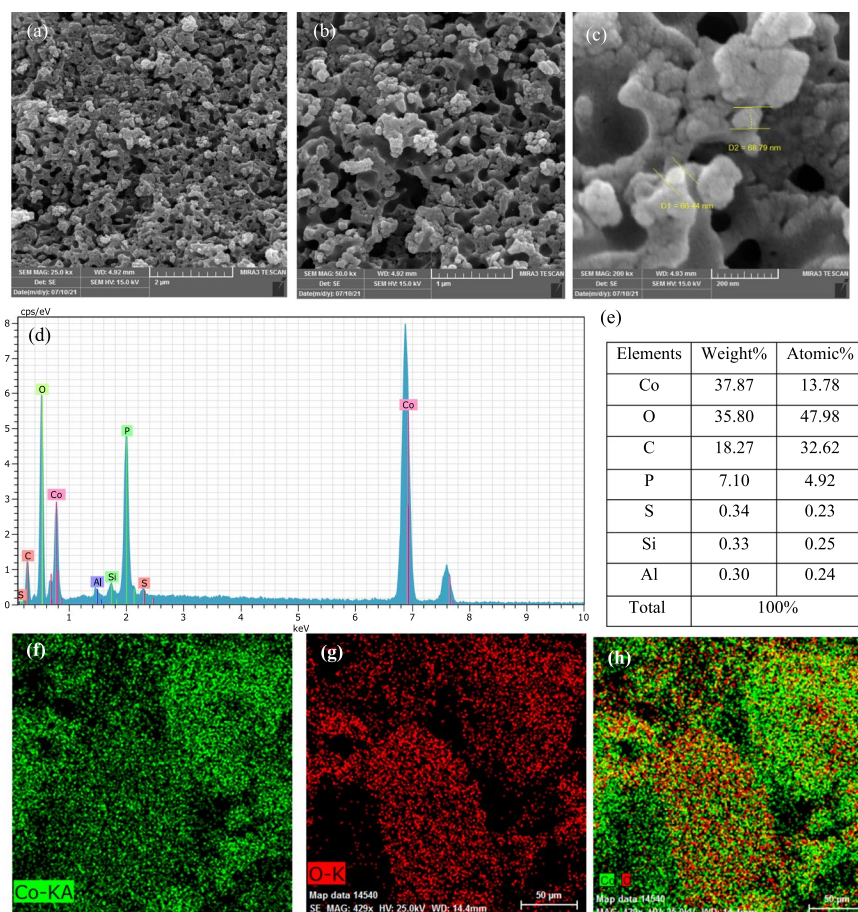


Fig. 3 FE-SEM micrographs, EDX spectrum, and elemental mapping micrographs of Co_3O_4 NPs. **a, b,** and **c** FE-SEM micrographs of biosynthesized Co_3O_4 NPs at different magnifications. **d, e** Types of elements, their weights, and atomic percentages in the sample of Co_3O_4 NPs produced using the biological method. **f–h** Elemental mapping image and abundance distribution of cobalt and oxygen elements in an electron microscope image. **(f)** Cobalt (Co) element, **(g)** Oxygen (O) element, and **(h)** cobalt oxide (CoO). The Co_3O_4 NPs exhibit a spherical shape and have an approximate size of 60 nm. They contain cobalt (Co) and oxygen (O) as major elements

ions, constituting over 70 percent of the entire sample, as well as other biological elements including phosphorus, carbon, silicon, sulfur, and aluminum. These findings indicated the successful biological synthesis of Co_3O_4 NPs. Signals corresponding to the characteristic binding energies of cobalt and oxygen were detected in the EDX spectrum (Fig. 3d, e). The agglomeration of nanoparticles can be attributed to the coating of biomolecules on their surface. Furthermore, elemental mapping analysis was conducted to assess the distribution of cobalt and oxygen elements in the scanning electron microscope image (Fig. 3f–h). The FTIR and EDX results indicated that the biological components present in the cellular extract of *Vibrio* sp. VLC played a crucial role as a reducing and stabilizing agent during the synthesis of Co_3O_4 NPs in this study. These components contributed to the successful formation and stability of the nanoparticles.

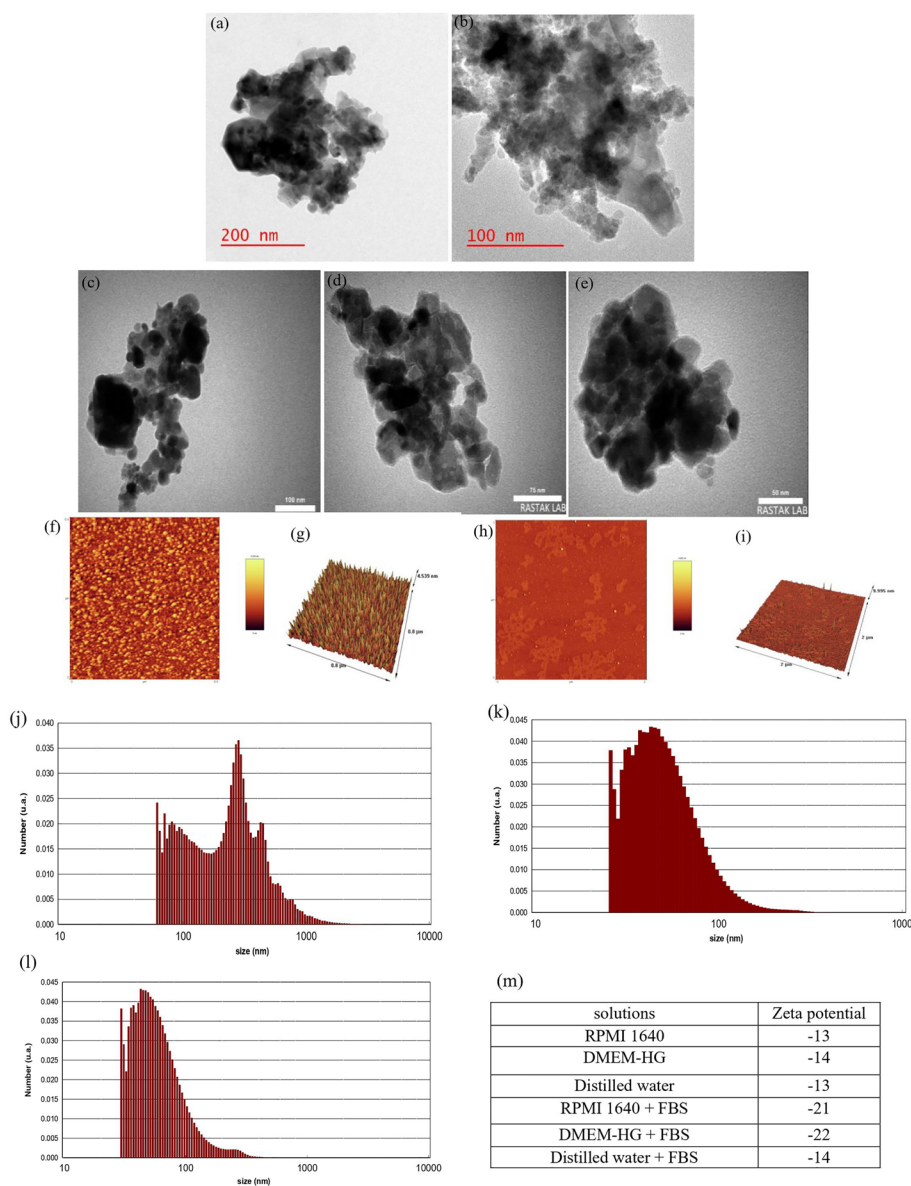


Fig. 4 Morphological analysis, AFM images, and particle size distribution of Co_3O_4 NPs. **a, b** Transmission electron microscopy (TEM) and **(c–e)** high resolution-transmission electron microscopy (HR-TEM) images of the NPs. **f, h** Represent 2D images, while **(g, i)** represent 3D images of Co_3O_4 NPs; **f, g** are on a scale of $0.8 \mu\text{m}$, and **(h, i)** are on a scale of $2 \mu\text{m}$. **j–l** Particle size distribution pattern in RPMI 1640, DMEM-HG, and water medium with the PDI of 0.22, 0.24, and 0.92, respectively. **m** Zeta potential of Co_3O_4 NPs in different solutions. Biosynthesized Co_3O_4 NPs are spherical particles ranging in size from 19 to 69 nm and their heights are reported to range from 4.5 to 10 nm

TEM, HR-TEM, AFM, DLS and zeta potential

To gain further insight into the particle size, shape, topography, surface, and average size of Co_3O_4 NPs produced using *Vibrio* sp. VLC bacteria extract, TEM, HR-TEM, AFM, DLS and zeta potential analyses were conducted (Fig. 4). The TEM micrographs revealed that the nanoparticles had a spherical morphology with an estimated size ranging from 32 to 69 nm (Fig. 4a, b). In order to achieve more precise measurements

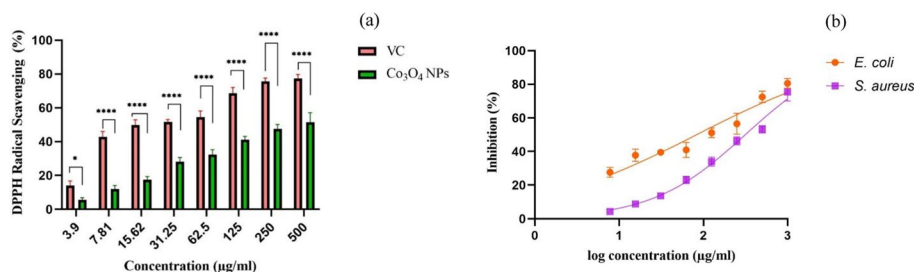


Fig. 5 Evaluation of antioxidant and antibacterial properties of Co₃O₄ NPs. **a** DPPH scavenging results for various concentrations of vitamin C and Co₃O₄ NPs. The DPPH inhibition was correlated with the concentrations of both vitamin C and Co₃O₄ NPs. The results are indicated as mean ± SD (*****p* < 0.0001). **b** Investigating the antibacterial properties of Co₃O₄ NPs on *E. coli* and *S. aureus* bacteria. The growth of both pathogenic bacteria was inhibited at all different concentrations of Co₃O₄ NPs. The results are indicated as mean ± SEM and the data are collected with 3 repetitions for each concentration

Table 1 Evaluating the antibacterial properties of Co₃O₄ NPs produced by biological method

Average percentage of survival related to <i>E. coli</i>								
Concentration (µg/ml)	7.81	15.62	31.12	62.5	125	250	500	1000
Average percentage of cell viability	73 ± 1.62	63 ± 1.76	62 ± 4.24	58 ± 1.3	48 ± 2.26	44 ± 0.24	28 ± 1.92	21 ± 1.1
Average percentage of survival related to <i>S. aureus</i>								
Concentration (µg/ml)	7.81	15.62	31.12	62.5	125	250	500	1000
Average percentage of cell viability	96 ± 2.13	91 ± 0.36	87 ± 0.81	78 ± 0.95	67 ± 0.31	54 ± 0.023	48 ± 0.30	28 ± 0.25

of the nanoparticles, high-resolution electron microscope images were also captured. The HR-TEM images indicated that the Co₃O₄ NPs had an approximate size within the range of 19 to 41 nm, while maintaining a spherical structure (Fig. 4c–e). The AFM micrographs also indicated that the nanoparticles had a predominantly spherical shape. The images revealed variations in height, as observed by the gradual transition from light to dark regions. Based on this study, the average height reported for Co₃O₄ NPs produced by the biological method was in the approximate range of 4.5 to 10 nm (Fig. 4f–i). Co₃O₄ NPs exhibited average sizes of 65 nm, 54 nm, and 270 nm when suspended in RPMI 1640, DMEM-HG, and water, respectively, based on DLS analysis (Fig. 4j–l). The nanoparticles demonstrated a monodisperse distribution in RPMI 1640 and DMEM-HG culture media, as indicated by the low polydispersity index (PDI). The zeta potential of Co₃O₄ NPs was measured in RPMI 1640, DMEM-HG, and distilled water, followed by visual examination of sedimentation rate after 24 h (Fig. 4m). The stability of cobalt oxide nanoparticles in these solvents, in combination with FBS, was also examined and the zeta potential results are mentioned in Fig. 4m. Accordingly, the zeta potential for nanoparticles increased in the presence of FBS. The stability of cobalt oxide nanoparticles in DMEM-HG + FBS (at a 1:1 ratio) had the highest level after 24 h.

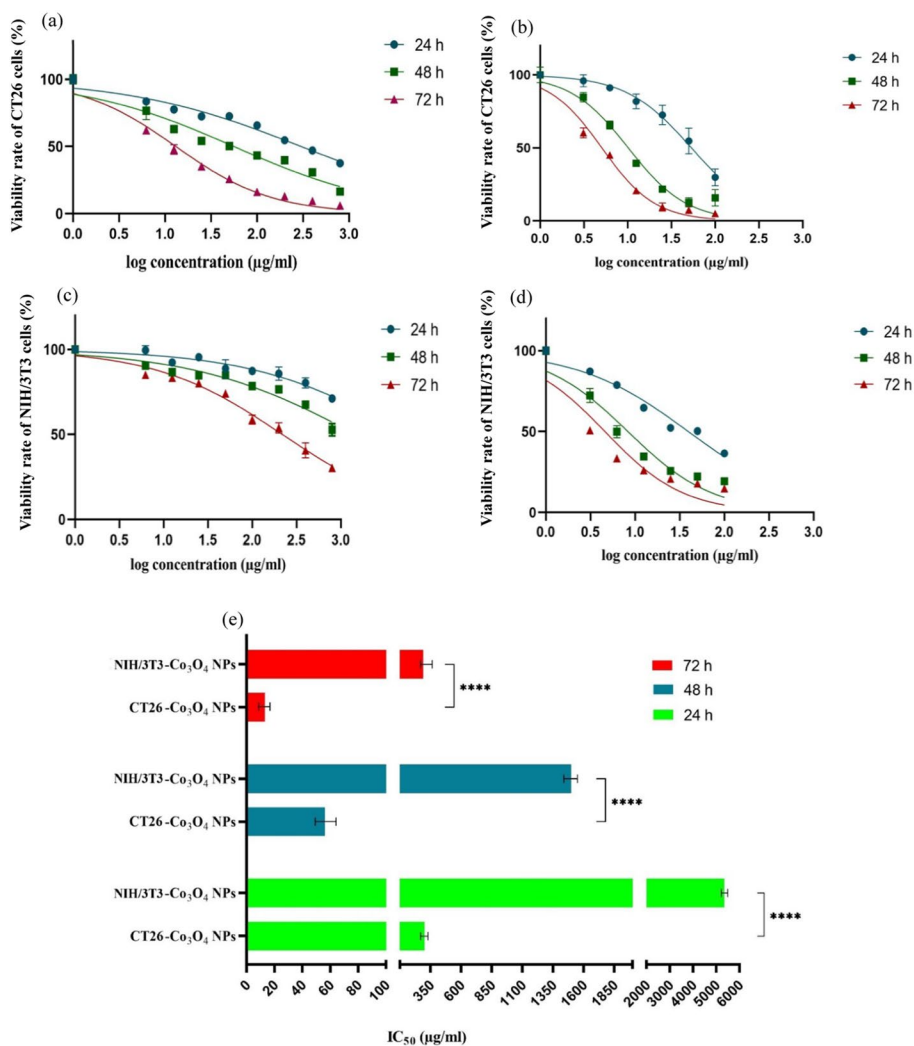


Fig. 6 Evaluating the cytotoxic effects of Co_3O_4 NPs synthesized using *Vibrio* sp VLC, and cisplatin on different cell lines. **a, c** Viability rate of CT26 and NIH/3T3 cells after exposing to different concentration of Co_3O_4 NPs, respectively. **b, d** Viability rate of CT26 and NIH/3T3 cells after exposing to different concentration of cisplatin, respectively. **e** Comparison between IC_{50} values of Co_3O_4 NPs on CT26 and NIH/3T3 cells at 24, 48, and 72 h. The results are indicated as mean \pm SD (**** $p < 0.0001$). The results demonstrated that the rate of inhibition and the percentage of cell viability decreased with increasing concentration and duration. Both Co_3O_4 NPs and cisplatin had strong inhibitory effects on CT26 cells, but Co_3O_4 NPs had a much smaller inhibitory effect on NIH/3T3 cells and were much less cytotoxic.

Antioxidant and antibacterial activity

In this study, the biological applications of Co_3O_4 NPs, including their antioxidant and antibacterial properties, were investigated. In order to evaluate the antioxidant properties, the ability of Co_3O_4 NPs to inhibit the DPPH radical was examined across 8 different concentrations. For comparative purposes, vitamin C (VC), a natural and potent antioxidant, was also included in the experiment. The highest rate of DPPH radical scavenging was observed at the concentration of $500 \mu\text{g/ml}$ for both Co_3O_4 NPs and vitamin C, resulting in approximately 51% and 78% inhibition, respectively. Furthermore, an increase in the concentrations of both nanoparticles and vitamin C led to a corresponding enhancement in DPPH inhibition (Fig. 5a). In addition, the

inhibitory potential of Co_3O_4 NPs at concentrations of 1000, 500, 250, 125, 62.5, 31.12, 15.62, and 7.81 $\mu\text{g}/\text{ml}$ against two pathogenic bacteria, namely *E. coli* and *S. aureus*, was investigated. Accordingly, the half-minimum inhibitory concentration (MIC_{50}) values for *E. coli* and *S. aureus* were determined to be 83 and 314 $\mu\text{g}/\text{ml}$, respectively (Fig. 5b). The percentage of bacterial growth inhibition was assessed across various nanoparticle concentrations as shown in Table 1.

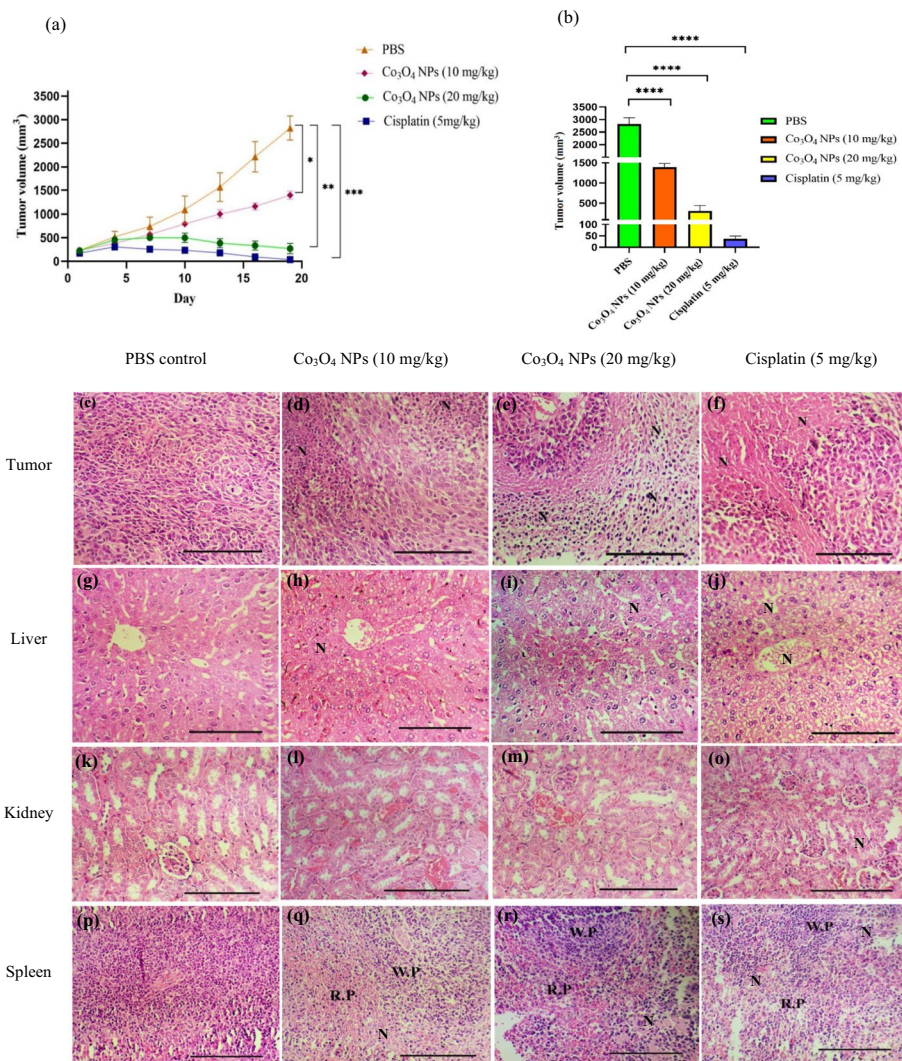


Fig. 7 In vivo and histopathological examination of the effects of Co_3O_4 NPs. **a** The average tumor volume variations after treatment with Co_3O_4 NPs (at 10 and 20 mg/kg concentrations), cisplatin (at 5 mg/kg concentration), and PBS on different days of treatment. The data are provided as mean \pm SEM (** $p < 0.001$). **b** Comparison between tumor volumes in different groups on the final day of the experiment. The values are provided as mean \pm SD (**** $p < 0.0001$). **c-s** Histopathological analysis of mice tumor tissues along with different organs (liver, kidney, and spleen) after 19 days exposure to Co_3O_4 NPs (at 10 and 20 mg/kg concentrations), cisplatin (at 5 mg/kg concentration), and PBS, (n = 5). PBS was demonstrated to be non-toxic, in all investigated tissues. Treatment with cisplatin and Co_3O_4 NPs at the concentration of 20 mg/kg led to the reduction and almost elimination of the induced colorectal tumors in mice, and in general, Co_3O_4 NPs caused less side effects in all the examined organs compared to the cisplatin. N indicates necrosis, W.P indicates white pulp, and R.P indicates red pulp. Scale bars represent 200 μm

Investigating the cytotoxicity of Co₃O₄ NPs and cisplatin on CT26 and NIH/3T3 cell lines

The impact of nanoparticles on cell viability was assessed by the MTT assay. Cisplatin was used as a control to better evaluate the cytotoxicity of the nanoparticles. The cell viability measurements were performed at 24, 48, and 72 h post-treatment. The findings indicated significant inhibitory effects of both nanoparticles and cisplatin on the growth of cancer cells. The inhibition rate of CT26 cells showed a direct correlation with two factors: the concentration of the compounds and the duration of the treatment. The IC₅₀ values of Co₃O₄ NPs at 24, 48, and 72 h were determined to be 301.8, 56.1, and 13.1 µg/ml, respectively. Moreover, the IC₅₀ values of cisplatin were found to be 39.8, 8.3, and 4.6 µg/ml at the corresponding time points (Fig. 6a, b).

The cytotoxicity induced with Co₃O₄ NPs and cisplatin on the NIH/3T3 cells was also investigated in this study. The IC₅₀ values of nanoparticles at 24, 48, and 72 h were 5356, 1498, and 291 µg/ml, respectively, whereas those for cisplatin were determined as 53.5, 10.1, and 5 µg/ml, respectively (Fig. 6c, d).

IC₅₀ comparison of Co₃O₄ NPs on cancerous vs normal cells

IC₅₀ values of Co₃O₄ NPs were investigated on both CT26 CRC cells and NIH/3T3 normal cells at 24, 48, and 72 h time intervals to assess the anti-cancer properties of the biosynthesized Co₃O₄ NPs (Fig. 6e). At 24 h, the IC₅₀ value of nanoparticles was 301.8 µg/ml for CT26 cells and 5356 µg/ml for NIH/3T3 cells, indicating a significant difference in the cytotoxic impact of Co₃O₄ NPs between cancerous and normal cells. After 48 h, the IC₅₀ values decreased to 56.1 µg/ml for CT26 cells and 1498 µg/ml for NIH/3T3 cells, and after 72 h, further dropped to 13.1 µg/ml and 291 µg/ml, respectively. These results indicate cell specific toxicity of Co₃O₄ NPs as they exhibited much lower inhibitory effects on the viability of NIH/3T3 cells.

Investigating the antitumor activity and the side effects of Co₃O₄ NPs in vivo

In order to investigate the in vivo antitumor activity of Co₃O₄ NPs synthesized through the biological method, BALB/c mice bearing CT26 tumors were intraperitoneally injected with 10 and 20 mg/kg Co₃O₄ NPs dispersed in PBS at 3 day intervals. Throughout the 19 day treatment period, the tumor volume was monitored (Fig. 7a). Additionally, a comparison was made between the tumor volumes at the end of the treatment period (Fig. 7b). The results demonstrated that both doses of Co₃O₄ NPs effectively suppressed tumor development. Notably, the administration of Co₃O₄ NPs at a dose of 20 mg/kg exhibited a comparable effect on tumor volume to that of cisplatin medication. The comparison of tumor volumes at the end of the treatment period revealed a significant inhibition of tumor growth in the groups treated with different concentrations of nanoparticles and cisplatin.

Histopathology evaluation

Based on the investigation conducted on tumor tissue sections obtained from mice subjected to various component concentrations, it was observed that all tissue sections exhibited malignant tumor cells of varying sizes (Fig. 7c–f). In the groups treated with cisplatin and 10 mg/kg of Co₃O₄ NPs, a substantial presence of necrotic

cells was observed. Additionally, the group treated with 20 mg/kg Co_3O_4 NPs displayed tumor cells with disorder and different sizes associated with necrosis. In the PBS-treated group, these phenomena were not prominently observed, and the tissues exhibited cells with enlarged and irregular nuclei. Thus, it can be inferred that the tumor tissue displayed an active nature and, to a certain extent, remained unaltered.

The group treated with cisplatin exhibited a notable presence of necrosis and tissue death in liver cells, along with hepatic congestion. Conversely, in the groups treated with 10 mg/kg and 20 mg/kg Co_3O_4 NPs, a minimal extent of necrosis and a minor degree of hepatic congestion were observed. In contrast, no tissue damage was observed in the group treated with PBS (Fig. 7g–j).

The histological examination of kidney tissue from mice treated with cisplatin revealed the presence of necrosis and structural alterations in the renal tubules. Additionally, the glomeruli displayed signs of contraction and compression, and the kidney tissue exhibited significant swelling. In contrast, while a few instances of renal congestion were observed in the groups treated with different doses of Co_3O_4 NPs, none of these cases was evident in the PBS-treated group (Fig. 7k–o).

Based on the histological examination of spleen tissue from mice administered with the respective compounds, the group treated with cisplatin displayed notable structural changes and necrosis in both the white and red pulps of the spleen. In contrast, the groups treated with two different concentrations of Co_3O_4 NPs exhibited only minor structural alterations in the white and red pulps of the spleen, while no damage was detected in the PBS-treated group. The administration of PBS demonstrated its expected non-toxicity, as assessed in the investigation of potential side effects on all the tissues (Fig. 7p–s).

Discussion

In the realm of specific cancer treatment, Co_3O_4 NPs have garnered considerable attention among various other nanoparticles. The biocompatibility of nanoparticles holds significant importance in biological applications, underscoring the need to carefully select an appropriate preparation method for obtaining biocompatible Co_3O_4 NPs. Presently, there is a limited body of research regarding the lethal concentrations of these nanoparticles on normal cells. While cobalt salts exhibit potent cytotoxic effects on all cell types, the utilization of Co_3O_4 NPs renders them specifically toxic to cancer cells. Utilizing biological sources for the synthesis of Co_3O_4 NPs has proved to be a safe, straightforward, and environmentally friendly approach (Caires et al. 2010; Huang et al. 2021; Iravani and Varma 2020; Hafeez et al. 2020; Govindasamy et al. 2022; Goswami et al. 2020).

In this study, a biological method utilizing the cell extract of *Vibrio* sp. VLC was employed for the synthesis of Co_3O_4 NPs. Among the three tested concentrations of $\text{Co}(\text{NO}_3)_2 \cdot 6\text{H}_2\text{O}$ salt (0.10, 0.15, and 0.20 mol/l), the 0.20 mol/l concentration proved to be more favorable for nanoparticle synthesis. This concentration exhibited superior efficiency while ensuring a size below 100 nm. The addition of the salt to the bacterial lysate extract resulted in the formation of cloudy compounds and violet-colored sediments, confirming the successful synthesis of nanoparticles. Similar research employed a Gram-positive bacterium (*Bacillus subtilis*) to biochemically produce Co_3O_4 NPs by

introducing $\text{CoCl}_2 \cdot 6\text{H}_2\text{O}$ salt into the bacterial medium. The addition of NaBH_4 as a reducing agent led to the initial color change and formation of sediments, indicating the progress of the synthesis process (Kalam *et al.* 2012). Additionally, Arsalan *et al.* reported the successful synthesis of Co_3O_4 NPs based on the color change observed when combining a pink cobalt chloride solution with a plant extract at concentrations of 0.10 and 0.20 mol/l (Arsalan *et al.* 2020).

As mentioned by Sanità *et al.*, biocompatibility is an important factor in the development of biosynthesized inorganic nanoparticles for biomedical applications. Various parameters influence the biocompatibility of a material, including its composition, intended use, desired biological response, and the environments it will encounter within the body. Surface modification strategies are crucial in enhancing the biocompatibility and cellular internalization of nanoparticles. Additionally, the introduction of pH-sensitive or heat-sensitive bonds has been explored to develop nanoplatforms for controlled drug release, specifically triggered by the acidity of tumor environment or external heat sources. The identification of Si, S, P, and Al in our environment of biosynthesized Co_3O_4 NPs underscores the biological synthesis method and the importance of thorough characterization in understanding the composition and potential influences on the nanoparticles properties and biocompatibility (Sanità *et al.* 2020; Saravanan *et al.* 2020; Abrishami *et al.* 2024a; Kamil Mohammad Al-Mosawi *et al.* 2023).

As argued by Choi & Lee, microbial cells play a significant role in the biosynthesis of inorganic nanoparticles, offering a green and sustainable alternative to conventional chemical and physical synthesis methods. These biological entities utilize various metabolic and physiological processes to reduce metal ions to their nanoparticle forms. The ability of these microorganisms to bind and reduce metal ions is attributed to the presence of specific proteins, enzymes, or biochemical pathways that facilitate the reduction process. These biosynthesized nanoparticles are of great interest for environmental remediation due to their enhanced reactivity, surface area, and the possibility of functionalization to target specific pollutants like heavy metals or organic contaminants. The biosynthetic method not only offers a more environmentally friendly approach of producing nanoparticles but also introduces the potential for creating novel nanoparticles with unique properties that might be difficult to achieve through other synthesis methods (Choi and Lee 2020; Saravanan *et al.* 2020).

Recent advancements in the field have focused on the preparation of biocompatible inorganic nanoparticles, bioconjugation strategies for target-specific nanoproboscopes, and the development of sensitive tumor imaging for diagnosis. These efforts underscore the complexity of nanoparticle behavior *in vivo*, influenced by their physicochemical properties and the interactions at the nano-bio interface. Based on the results of *in vivo* research, the biosynthesized Co_3O_4 NPs exhibited targeted damage to cancerous cells within tumor tissue, with the lowest level of damage observed in other tissues. The challenges ahead involve better understanding these interactions and designing nanoparticles that can safely and effectively be used in clinical settings (Jiao *et al.* 2018; Saravanan *et al.* 2020).

Characterization of biosynthesized Co_3O_4 NPs

The XRD analysis revealed distinct 2θ values of 20.05 (111), 31.19 (220), 36.56 (311), and 44.29 (400), which coincided with the JCPDS pattern No. 073–1701 for spherical Co_3O_4 NPs. This agreement confirms the successful synthesis of Co_3O_4 NPs. Notably, the absence of specific peaks in the XRD spectrum of unheated nanoparticles indicates their amorphous nature and the presence of various impurities. Conversely, the sharp peaks observed in the XRD spectrum of the sample annealed at 600 °C, compared to the weaker peaks for the sample heated at 500 °C, indicated a reduction in impurities and the crystallization of the nanoparticles. Previous studies also examined XRD results to confirm the production and assessed the crystallization of Co_3O_4 NPs by evaluating the similarity and absence of additional peaks when compared to registered cases (Yang et al. 2015; Das and Saikia 2023; Bechelany et al. 2010; Vijayanandan and Balakrishnan 2018; Bibi et al. 2017; Kumar et al. 2008). In order to confirm the successful synthesis of Co_3O_4 NPs using the *Vibrio* extract, the FTIR spectra of both unheated and heated samples were compared with similar studies. The unheated sample exhibited prominent peaks in the wave number region associated with amino, amide, and hydrocarbon compounds. These peaks can be attributed to the presence of enzyme residues and proteins in the bacterial extract, which strongly supports the biological production of the nanoparticles (Vijayanandan and Balakrishnan 2018; Eid 2022; Farhadi et al. 2013; Naumann et al. 1991).

The EDX analysis revealed that the biologically synthesized sample had an elemental composition consisting of cobalt and oxygen, which accounted for more than 70% of the total composition. This high percentage signifies the high purity of the produced nanoparticles. Additionally, a small percentage of phosphorus, carbon, and sulfur elements was detected, indicating the presence of biological compounds during the production process. In a similar study conducted by Akhlaghi et al., green Co_3O_4 NPs were successfully produced with an acceptable purity percentage of cobalt and oxygen elements, reaching up to approximately 60% of the total composition (Akhlaghi et al. 2020).

To examine the size and shape characteristics of cobalt oxide NPs, multiple imaging techniques were employed including TEM, HR-TEM, FE-SEM, AFM, and DLS. Analyzing the micrographs revealed that Co_3O_4 NPs exhibited a spherical morphology, with sizes ranging from 20 to 70 nm (less than 100 nm). These findings are consistent with recent research, which also reported similar observations regarding the shape and size of Co_3O_4 NPs (Rousta et al. 2019; Abbasi et al. 2020; Bibi et al. 2017; Ajarem et al. 2021; Mehrafza et al. 2022; Vijayanandan and Balakrishnan 2018; Jang et al. 2015).

The physical properties of Co_3O_4 nanoparticles, specifically size, polydispersity index (PDI), and zeta potential, greatly influence their biological activities. The DLS analysis revealed that the nanoparticles exhibit a narrow size distribution, which is required for their interaction with biological systems, where smaller particles are known to penetrate cell membranes more efficiently, potentially enhancing their anticancer activity. Moreover, the zeta potential values obtained for these nanoparticles in various media indicate a stable colloidal system, which is vital for maintaining the dispersion of nanoparticles in biological environments. The negative zeta potential values, especially in the presence of FBS, suggest that the nanoparticles are likely to repel each other, preventing aggregation (AlSalhi et al. 2024).

The integration of DLS and zeta potential results into our biological findings allows us to hypothesize the mechanisms through which these characteristics enhance the effectiveness of Co_3O_4 NPs. The optimized size and stable dispersion contribute to the nanoparticles ability to induce oxidative stress within cancer cells effectively, without causing significant harm to normal cells. This selective toxicity towards cancer cells can be attributed to the nanoparticles enhanced penetration and retention within the tumor tissues, a phenomenon often referred to as the enhanced permeability and retention (EPR) effect. Furthermore, the surface charge indicated by the zeta potential might influence the interaction of nanoparticles with cell membranes, potentially affecting the cellular uptake and the subsequent intracellular pathways activated by the nanoparticles. This could explain the observed variations in antioxidant, antibacterial, and anticancer activities, as the interaction dynamics between nanoparticles and cellular components are crucial determinants of their biological effects. DLS and zeta potential analyses conducted in this study revealed that our nanoparticles exhibit a highly uniform size distribution with average diameters of 65 nm in RPMI 1640, 54 nm in DMEM-HG,, and an unusually large size of 270 nm in distilled water, alongside stable zeta potential values indicative of colloidal stability in various media, which was enhanced by FBS (Kavitha et al. 2017).

Saravanan et al. discussed the impact of secondary metabolite conjugation on the biological activity of inorganic nanoparticles, focusing on modulating their effects for therapeutic use. Conjugating bioactive compounds from microorganisms, fungi, or plants with nanoparticles enhances their biological activity and specificity. This process can improve therapeutic potential, by increased solubility and bioavailability when attached to gold nanoparticles, enhancing their anti-cancer efficacy. Selecting appropriate natural resources for nanoparticle synthesis is crucial, especially for targeting specific therapeutic outcomes, allowing for the design of nanoparticles with enhanced activity, like those with anticancer properties. This method of integrating secondary metabolites with specific therapeutic profiles into nanoparticle design fosters the development of targeted and effective nanotherapeutics, leveraging natural compound benefits for targeted treatment while minimizing side effects (Saravanan et al. 2021).

Furthermore, biological methods for fabricating metal nanoparticles are increasingly favored over traditional physical and chemical techniques due to their alignment with green chemistry and sustainability principles. These methods are energy-efficient, often requiring only ambient conditions, and produce biocompatible nanoparticles without the need for harmful chemicals or extensive modifications. The biological methods not only avoid toxic by-products but also offer enhanced stability and dispersion of nanoparticles through natural capping agents. Furthermore, biological synthesis is cost-effective, scalable, and typically involves simpler, single-step processes, making it suitable for large-scale production. While acknowledging that each synthesis method has its pros and cons based on the application needs, the emphasis on sustainability, safety, and biocompatibility continues to drive the preference for biological approaches in nanoparticle synthesis (Samadian et al. 2020; Vahidi et al. 2021).

The influence of characteristic parameters on the biological interactions of nanomaterials

Samadian et al. emphasized the significant impact of various nanoparticle properties (such as shape, size, surface charge, and chemical composition) on their biological behavior and therapeutic potential. The size of nanoparticles not only determines their cellular uptake efficiency but also their distribution within the body, including the ability to cross the biological barriers such as the blood–brain barrier. The geometry of nanoparticles affects their internalization by cells and their subsequent intracellular fate. The shape also influences the ability of nanoparticles to navigate through the extracellular matrix and their interactions with cell membranes, potentially affecting their ability to reach target sites within the body. Nanoparticles in the range of 1–100 nm can take advantage of unique size-dependent properties not seen in their bulk material counterparts (Albanese et al. 2012; Samadian et al. 2020).

The dissolution and agglomeration behaviors of nanoparticles further dictate their bioavailability and therapeutic effectiveness. Faster-dissolving nanoparticles may release therapeutic ions more rapidly, leading to quicker biological responses. However, this can also mean a higher potential for toxicity if the released ions exceed safe concentration thresholds. The solubility of nanoparticles is influenced by factors such as pH, ionic strength of the solution, and the presence of biomolecules, which can either facilitate or inhibit dissolution. Agglomeration can significantly reduce the surface area available for interaction with biological molecules, potentially diminishing the reactivity and efficacy of nanoparticles. Moreover, larger agglomerates might be less efficiently taken up by cells and may be more readily cleared from the body, impacting the delivery efficiency of the therapeutic nanoparticles (Samadian et al. 2020; Godymchuk et al. 2022; Avramescu et al. 2022). Moreover, specific surface area and surface properties, including morphology, energy, coating, and charge, are crucial for enhancing interactions with biological systems, requiring meticulous design to enhance efficacy while minimizing adverse reactions (Samadian et al. 2020; Joudeh and Linke 2022).

As pointed out by Hu et al., the topography of the surface of a nanoparticle, including its roughness or smoothness, can also influence protein adsorption patterns and cellular interactions. Rees et al. argue that coating nanoparticles with biocompatible materials (e.g., polyethylene glycol, dextran, or lipids) can significantly reduce unspecific protein adsorption, minimizing recognition by the immune system and prolonging circulation time in the bloodstream. These coatings can also be functionalized with targeting ligands or antibodies to achieve specific binding to target cells or tissues, improving the efficacy of drug delivery or imaging. This comprehensive understanding underscores the importance of tailoring nanoparticle properties to harness their full potential in medical applications (Hu et al. 2022; Rees et al. 2019; Samadian et al. 2020).

Antioxidant and antibacterial activity

The antioxidant activity of Co_3O_4 NPs was investigated by assessing their ability to reduce the DPPH free radical. As a comparative reference, vitamin C, a potent natural antioxidant, was used as a positive control. At the highest concentration tested (500 $\mu\text{g}/\text{ml}$), both Co_3O_4 nanoparticles and vitamin C exhibited significant reductions in DPPH, with values of 51.24% and 77.54%, respectively. These findings indicate that the antioxidant activity strengthens with increasing the nanoparticle concentration.

Based on the results of the MIC test, the concentrations of Co_3O_4 NPs utilized in this study exhibited antibacterial effects and inhibited the growth of both *E. coli* and *S. aureus* bacteria. Notably, the inhibition observed on *E. coli* was stronger compared to *S. aureus*. This difference in susceptibility could potentially be attributed to the variations in cell wall structures between Gram-negative and Gram-positive bacteria, with Gram-negative bacteria possessing relatively thinner cell walls (Moradpoor et al. 2019). Moreover, the unique properties of Co_3O_4 NPs, such as their ability to generate and release oxygen radicals, can induce greater stress specifically on Gram-negative bacteria (Abbasi et al. 2020; Gupta et al. 2020; Azam et al. 2012). The MIC_{50} values of Co_3O_4 NPs synthesized using the biological method were determined to be 83 $\mu\text{g}/\text{ml}$ for *E. coli* and 314 $\mu\text{g}/\text{ml}$ for *S. aureus* bacteria. Other studies have also demonstrated that the antioxidant and antibacterial properties of Co_3O_4 nanoparticles enhance as their concentrations increase (Ajarem et al. 2021; Brand-Williams et al. 1995; Khalil et al. 2020; Khan et al. 2015; Hou et al. 2020).

In vitro and in vivo studies

The use of chemotherapy drugs, including cisplatin, has become a common approach for treating different types of cancers. However, studies have indicated that cisplatin can heighten the susceptibility of mitochondria to reactive oxygen species (ROS), resulting in oxidative damage to normal cells. Prolonged exposure to oxidative stress can lead to organ dysfunction, particularly affecting the kidney, liver, and spleen. Consequently, it is of paramount importance to enhance treatment efficacy and minimize the long-term side effects associated with the use of cisplatin in cancer therapy (Ertugrul et al. 2020; Mishra et al. 2017; Taléns-Visconti et al. 2022).

The cytotoxicity of Co_3O_4 NPs was assessed by the MTT assay at 24, 48, and 72 h following the exposure of CT26 and NIH/3T3 cells to the nanoparticles. The cytotoxicity of Co_3O_4 NPs on the NIH/3T3 cells exhibited an enhanced trend with increasing concentrations, but did not induce a significant toxicity. In line with previous research findings, these nanoparticles demonstrated lower toxicity towards normal cells. However, Co_3O_4 NPs exerted distinct lethal effects on CT26 CRC cells. The results revealed an inverse relationship between CT26 cells viability and the duration and dosage of Co_3O_4 nanoparticles. The IC_{50} values of Co_3O_4 nanoparticles on the CT26 cells were determined to be 301.8, 56.1, and 13.1 $\mu\text{g}/\text{ml}$ after 24, 48, and 72 h of exposure, respectively. This research underscores the potential cytotoxicity of Co_3O_4 NPs towards CT26 CRC cells. By comparing the IC_{50} values of Co_3O_4 NPs on CT26 and NIH/3T3 cell lines, it can be inferred that these nanoparticles exhibited minimal toxicity towards normal cells at the comparable concentrations and exposure durations. Additionally, the IC_{50} values of cisplatin further validated its high toxicity on both the CT26 CRC and NIH/3T3 normal cells. There were no significant changes in the survival percentages of the two cell lines after 48 and 72 h of cisplatin treatment. The selective toxicity of nanoparticles on CRC cells compared to normal cells was demonstrated by comparing the survival percentages of CT26 and NIH/3T3 cells treated with Co_3O_4 NPs and cisplatin at the equivalent concentrations of both substances after 24, 48, and 72 h of treatment. Khan et al. conducted a similar study, and investigated the cytotoxicity of Co_3O_4 NPs, synthesized using a semi-biological method, on human CRC cells (HT-29 and SWC620).

Their findings revealed that these nanoparticles exhibited a favorable cytotoxic profile compared to doxorubicin, and induced minimal cytotoxicity on normal cells. This highlights their potential as a toxic agent specifically targeting cancerous cells (Khan et al. 2015). Moreover, an examination of the effects of Co_3O_4 NPs, produced using biological compounds, was performed on human leukemia cells. The study showed that these NPs exhibited a controlled toxic effect on cancerous cells, while maintaining a higher cell viability percentage in normal cells. These findings further support the notion of the selective toxicity of Co_3O_4 NPs towards cancerous cells compared to normal cells (Chattopadhyay et al. 2014a). Co_3O_4 NPs exert cell damage through two main mechanisms. Firstly, the presence of Co^{2+} ions leads to DNA damage and fragmentation by binding to the nucleosome. Secondly, these nanoparticles play a crucial role in inducing apoptosis through the generation of ROS (Faisal et al. 2016; Bhatia et al. 2022; He et al. 2018; Tripathi et al. 2019; Iqbal et al. 2020; Chattopadhyay et al. 2014b; Ajarem et al. 2021). The reductive property of biological Co_3O_4 NPs is more pronounced in an acidic environment compared to a neutral environment. These nanoparticles exhibit a remarkable ability to penetrate cancerous cells in large quantities, facilitated by the higher concentration of phospholipids in the membrane of cancerous cells. Consequently, this leads to a substantial release of Co^{2+} ions and a heightened formation of ROS within cancerous cells, surpassing that observed in normal cells. This process increases the production of ROS and causes cell apoptosis by increasing the expression of pro-apoptotic proteins like P53, Caspase 3, and Caspase 8. Our research indicates that Co_3O_4 NPs synthesized using *Vibrio* sp. VLC exhibit comparable high selective toxicity against cancerous cells, in alignment with findings from earlier studies on nanoparticles synthesized via biological methods (Iqbal et al. 2020; Huang et al. 2021; Ajarem et al. 2021; Khan et al. 2015; Chattopadhyay et al. 2014b).

Our study meticulously investigated the dose-dependent effects of Co_3O_4 NPs on tumor growth and tissue morphology, revealing significant insights into their therapeutic potential. Administering Co_3O_4 NPs at doses of 10 and 20 mg/kg to BALB/c mice bearing CT26 tumors led to a notable suppression of tumor development, illustrating a clear dose-dependent efficacy. Particularly, the 20 mg/kg dosage of Co_3O_4 NPs demonstrated a tumor volume reduction comparable to that achieved with cisplatin treatment, a conventional chemotherapy drug, underscoring the potent anticancer properties of Co_3O_4 NPs. Histopathological evaluation further substantiated these findings, as tissue sections from treated mice showcased varying degrees of malignant cell necrosis, dependent on the NPs dosage. The higher dose (20 mg/kg) resulted in more pronounced necrotic changes within tumor cells, indicative of increased therapeutic efficacy. Comparatively, the histopathology results mirror findings from similar nanoparticle research, such as the study of Kavaz, where metal oxide nanoparticles also exhibited dose-dependent anticancer activities through mechanisms like ROS generation and DNA damage. Similarly, Nakhaeipour et al. noted a dose-dependent cytotoxic effect of biogenic CuO NPs, highlighting their safer production and use. This underscores the consistency of Co_3O_4 NPs effects across different experimental frameworks and supports their potential utility in targeted cancer therapy. Furthermore, the minimal histological alterations observed in non-tumoral tissues treated with Co_3O_4 NP, especially compared to widespread tissue damage of cisplatin, highlight the superior safety profile of these nanoparticles (Kavaz

et al. 2021; Chattopadhyay et al. 2014b; Nakhaeepour et al. 2019). Comparing the tumor volumes of mice at the end of the treatment period demonstrated a significant inhibition of tumor growth in the groups treated with various concentrations of Co_3O_4 NPs and cisplatin. Specifically, cisplatin resulted in a notable reduction and nearly complete elimination of the induced mouse colorectal tumor. Moreover, the concentration of 10 mg/kg Co_3O_4 NPs effectively impeded the growth of the mouse colorectal tumor, in contrast to the control group treated with PBS. These findings highlight the potential of 20 mg/kg Co_3O_4 NPs as a promising alternative to cisplatin, while also indicating the inhibitory effect of 10 mg/kg Co_3O_4 NPs on tumor growth. The method for administration of nanoparticles varies depending on their characteristics such as nature, size, and shape. Due to the potential hemolytic activity associated with high concentrations of Co_3O_4 NPs, intraperitoneal or subcutaneous injections have been utilized in previous studies (Chattopadhyay et al. 2014a, 2013; Ajarem et al. 2021; Huang et al. 2021). Our histological data analysis demonstrated that cisplatin, aside from its potent anticancer properties, induced significant tissue damage in the liver, kidney, and spleen. In contrast, the application of Co_3O_4 NPs at both concentrations did not cause tissue damage in the spleen and exhibited minimal damage in liver and kidney tissues (Gong et al. 2021; Ertugrul et al. 2020). The presence of necrosis in liver cells and in the white and red pulps of the spleen after cisplatin treatment align with the cytotoxic effects. The minimal extent of necrosis and hepatic congestion, observed in the groups treated with Co_3O_4 NPs suggests a potentially lower cytotoxic effect compared to cisplatin. Additionally, the absence of renal congestion in the PBS-treated group and the presence of minimal renal congestion in the groups treated with Co_3O_4 NPs suggest a potential difference in renal toxicity between the treatments. The structural alterations in renal tubules, glomerular contraction, compression, and significant swelling of kidney tissue after cisplatin treatment align with similar findings after exposure to ZnO NPs and cisplatin. Moreover, the disorder and different sizes of tumor cells associated with necrosis in the group treated with 20 mg/kg Co_3O_4 NPs align with the concentration-dependent effect observed in the Kavaz et al. research, where higher concentrations of ZnO NPs induced morphological alterations in tissues (Kavaz et al. 2021).

Furthermore, in the context of exploring sustainable methods for nanoparticle synthesis, the findings of this study on Co_3O_4 nanoparticles synthesized via biological routes contribute to a broader understanding of green nanotechnology. The capability of biological approaches to fabricate diverse metal-based nanoparticles, was also demonstrated across various studies, in the synthesis of zinc oxide nanoparticles (Ahmed et al. 2021), zirconium nanoparticles (Golnaraghi Ghomi et al. 2019), and tellurium nanoparticles (Vahidi et al. 2021).

Conclusion

In this study, we explored the use of Co_3O_4 NPs synthesized using *Vibrio* sp. VLC for CRC therapy. Through methods like XRD, EDX, and FTIR analyses, we established their spherical morphology and analyzed their physicochemical properties. Our investigations into the effects of Co_3O_4 NPs on CRC cells and normal NIH/3T3 cells revealed a notable anticancer activity against CRC cells, suggesting a potential for therapeutic

applications. The NPs were also found to possess antioxidant and antibacterial properties and to selectively induce apoptosis in CT26 CRC cells.

Compared with cisplatin, a standard medicine in cancer treatment, biosynthesized Co_3O_4 NPs showed a promising tumor growth inhibition in a mouse model with less toxicity towards vital organs. This outcome underscores the potential of Co_3O_4 NPs to reduce the side effects commonly associated with traditional chemotherapy, though it is crucial to note that these findings are preliminary.

The synthesis method utilizing *Vibrio* sp. VLC highlights an area of interest for nanoparticle fabrication, suggesting a direction for future research in safer and possibly more targeted cancer treatments. Yet, it is important to proceed with further studies to understand the mechanisms through which Co_3O_4 NPs exert their effects and to verify their safety and effectiveness in more complex biological models.

Our findings contribute to the growing body of research on nanotechnology in cancer therapy. They underscore the importance of continued exploration in this area, particularly for treatments that aim to be less toxic and more targeted. Future research should focus on enhancing nanoparticle delivery mechanisms and conducting comprehensive clinical trials to assess the practical benefits of Co_3O_4 NPs in colorectal cancer therapy.

Abbreviations

AFM	Atomic force microscopy
Co_3O_4 NPs	Cobalt oxide nanoparticles
CRC	Colorectal cancer
DMSO	Dimethyl sulfoxide
DMEM-HG	Dulbecco's modified Eagle's medium–high glucose
DLS	Dynamic light scattering
DPPH	1,1-Diphenyl-2-picrylhydrazyl
EDX	Energy-dispersive X-ray spectroscopy
<i>E. coli</i>	<i>Escherichia coli</i>
FBS	Fetal bovine serum
FE-SEM	Field emission-scanning electron microscopy
FTIR	Fourier-transform infrared
FWHM	Full width at half maximum
H&E	Hematoxylin and eosin
HR-TEM	High resolution-transmission electron microscopy
MIC	Minimum inhibitory concentration
MTT	3-[4,5-Dimethylthiazole-2-yl]-2,5-diphenyltetrazolium bromide
ROS	Reactive oxygen species
PBS	Phosphate-buffered saline
RPMI	Roswell Park Memorial Institute
SWC	Sea water complex
<i>S. aureus</i>	<i>Staphylococcus aureus</i>
TEM	Transmission electron microscopy
XRD	X-ray diffraction

Acknowledgements

The authors would like to thank Mohammad Mesgari, Mohammad Hassan Mollaei, Amir Abrishami, Niloufar Hosseini Giv, and Sepehr Attaran for their excellent support and technical assistance. Additionally, we would like to acknowledge Central Lab Facility of Ferdowsi University of Mashhad and Parsian Medical Laboratory Center for their cooperation and technical support.

Author contributions

FME was responsible for investigation, data curation, methodology, software utilization, and writing the original draft. MM contributions included supervision, conceptualization, validation, funding acquisition, and resource provision. MMM contributed to project administration, supervision, conceptualization, validation, funding acquisition, methodology, resource provision, and manuscript text writing, reviewing, and editing. All authors participated in the manuscript review process.

Funding

This work was supported by Ferdowsi University of Mashhad, grant number: 57277.

Availability of data and materials

All data generated or analyzed during this study are included in this article and additional data are available from the corresponding author upon reasonable request.

Declarations

Ethics approval and consent to participate

This research was approved by the ethics committee at Ferdowsi University of Mashhad (approval number: IR.UM.REC.1401.01).

Consent for publication

Not applicable.

Competing interests

The authors declare that they have no competing interests.

Received: 20 January 2024 Accepted: 28 March 2024

Published online: 05 April 2024

References

- Abbasi BA, Iqbal J, Khan Z, Ahmad R, Uddin S, Shahbaz A, Zahra SA, Shaikat M, Kiran F, Kanwal S, Mahmood T (2020) Phytofabrication of cobalt oxide nanoparticles from *Rhamnus virgata* leaves extract and investigation of different bioactivities. *Microsc Res Tech* 84(2):192–201. <https://doi.org/10.1002/jemt.23577>
- Abdurakhmonov OE, Alisultanov ME, Vertaeva DA, Muradova AG (2022) The effect of annealing temperature on crystallization of Nd_2O_3 nanoparticles synthesized by the deposition method. *Inorg Chem* 67(7):1118–1124. <https://doi.org/10.1134/s0036023622070026>
- Abrishami A, Bahrami AR, Nekooei S, Sh Saljooghi A, Matin M (2024a) Hybridized quantum dot, silica, and gold nanoparticles for targeted chemo-radiotherapy in colorectal cancer theranostics. *Commun Biol* 7(1): 1–19. <https://doi.org/10.1038/s42003-024-06043-6>
- Abrishami A, Bahrami AR, Saljooghi AS, Matin, MM (2024b) Enhanced theranostic efficacy of epirubicin-loaded SPION@MSN through co-delivery of an anti-miR-21-expressing plasmid and ZIF-8 hybridization to target colon adenocarcinoma. *Nanoscale* 16(12):6215–6240. <https://doi.org/10.1039/d3nr06642h>
- Ahmed Rather G, Nanda A, Ahmad Pandit M, Yahya S, Sofi MA, Barabadi H, Saravanan M (2021) Biosynthesis of zinc oxide nanoparticles using *Bergenia ciliata aqueous* extract and evaluation of their photocatalytic and antioxidant potential. *Inorganic Chem Commun* 134:109020. <https://doi.org/10.1016/j.inoche.2021.109020>
- Ajarem JS, Maooda SN, Allam AA, Taher MM, Khalaf M (2021) Benign synthesis of cobalt oxide nanoparticles containing red algae extract: antioxidant, antimicrobial, anticancer, and anticoagulant activity. *Cluster Sci* 33(2):717–728. <https://doi.org/10.1007/s10876-021-02004-9>
- Akhlaghi N, Najafpour-Darzi G, Younesi H (2020) Facile and green synthesis of cobalt oxide nanoparticles using ethanolic extract of *Trigonella Foenumgraceum* (Fenugreek) leaves. *Adv Powder Technol* 31(8):3562–3569. <https://doi.org/10.1016/j.apt.2020.07.004>
- Albanese A, Tang PS, Chan WCW (2012) The effect of nanoparticle size, shape, and surface chemistry on biological systems. *Annu Rev Biomed Eng* 14(1):1–16. <https://doi.org/10.1146/annurev-bioeng-071811-150124>
- AlSalhi MS, Oza G, Castillo-Maldonado I, Sharma A (2024) Evaluation of antimicrobial, antioxidant, and anti-inflammatory abilities of sustainably synthesized Co_3O_4 NPs. *Biocatal Agric Biotechnol* 56:103025. <https://doi.org/10.1016/j.bcab.2024.103025>
- Arghiani N, Matin MM, Bahrami AR, Iranshahi M, Sazgarnia A, Rassouli FB (2014) Investigating anticancer properties of the sesquiterpene ferutinol on colon carcinoma cells, in vitro and in vivo. *Life Sci* 109(2):87–94. <https://doi.org/10.1016/j.lfs.2014.06.006>
- Arsalan N, Hassan Kashi E, Hasan A, Edalat Doost M, Rasti B, Ahamad Paray B, Zahed Nakhjiri M, Sari S, Sharifi M, Shahpasand K, Akhtari K, Haghghat S, Falahati M (2020) Exploring the interaction of cobalt oxide nanoparticles with albumin, leukemia cancer cells and pathogenic bacteria by multispectroscopic, docking, cellular and antibacterial approaches. *Nanomedicine* 15:4607–4623. <https://doi.org/10.2147/IJN.S257711>
- Avramescu M-L, Chénier M, Beauchemin S, Rasmussen PE (2022) Dissolution behaviour of metal-oxide nanomaterials in various biological media. *Nanomaterials* 13(1):26. <https://doi.org/10.3390/nano13010026>
- Azam A, Ahmed AS, Oves M, Khan MS, Habib SS, Memic A (2012) Antimicrobial activity of metal oxide nanoparticles against Gram-positive and Gram-negative bacteria: a comparative study. *Nanomedicine* 7:6003–6009. <https://doi.org/10.2147/IJN.S35347>
- Bechelany M, Maeder X, Riesterer J, Hankache J, Lerosé D, Christiansen S, Michler J, Philippe L (2010) Synthesis mechanisms of organized gold nanoparticles: influence of annealing temperature and atmosphere. *Cryst Growth Des* 10(2):587–596. <https://doi.org/10.1021/cg900981q>
- Bhatia SN, Chen X, Dobrovolskaia MA, Lammers T (2022) Cancer nanomedicine. *Nat Rev Cancer* 22(10):550–556. <https://doi.org/10.1038/s41568-022-00496-9>
- Bibi I, Nazar N, Iqbal M, Kamal S, Nawaz H, Nouren S, Safa Y, Jilani K, Sultan M, Ata S, Rehman F, Abbas M (2017) Green and eco-friendly synthesis of cobalt-oxide nanoparticle: characterization and photo-catalytic activity. *Adv Powder Technol* 28(9):2035–2043. <https://doi.org/10.1016/j.apt.2017.05.008>

- Brand-Williams W, Cuvelier ME, Berset C (1995) Use of a free radical method to evaluate antioxidant activity. *LWT Food Sci Technol* 28(1):25–30. [https://doi.org/10.1016/s0023-6438\(95\)80008-5](https://doi.org/10.1016/s0023-6438(95)80008-5)
- Caires FJ, Lima LS, Carvalho CT, Ionashiro M (2010) Thermal behaviour of succinic acid, sodium succinate and its compounds with some bivalent transition metal ions. *Thermochim Acta* 500(1–2):6–12. <https://doi.org/10.1016/j.tca.2009.11.015>
- Chattopadhyay S, Dash SK, Ghosh T, Das D, Pramanik P, Roy S (2013) Surface modification of cobalt oxide nanoparticles using phosphonomethyl iminodiacetic acid followed by folic acid: a biocompatible vehicle for targeted anticancer drug delivery. *Cancer Nanotechnol* 4(4–5):103–116. <https://doi.org/10.1007/s12645-013-0042-7>
- Chattopadhyay S, Dash SK, Kar Mahapatra S, Tripathy S, Ghosh T, Das B, Das D, Pramanik P, Roy S (2014a) Chitosan-modified cobalt oxide nanoparticles stimulate TNF- α -mediated apoptosis in human leukemic cells. *Bio Inorgan Chem* 19(3):399–414. <https://doi.org/10.1007/s00775-013-1085-2>
- Chattopadhyay S, Dash SK, Tripathy S, Pramanik P, Roy S (2014b) Phosphonomethyl iminodiacetic acid-conjugated cobalt oxide nanoparticles liberate Co^{2+} ion-induced stress associated activation of TNF- α /p38 MAPK/caspase 8-caspase 3 signaling in human leukemia cells. *Bio Inorgan Chem* 20(1):123–141. <https://doi.org/10.1007/s00775-014-1221-7>
- Chen L, Zhu Y, Yang D, Zou R, Wu J, Tian H (2014) Synthesis and antibacterial activities of antibacterial peptides with a spiropyran fluorescence probe. *Sci Rep* 4:6860. <https://doi.org/10.1038/srep06860>
- Choi Y, Lee SY (2020) Biosynthesis of inorganic nanomaterials using microbial cells and bacteriophages. *Nat Rev Chem* 4(12):638–656. <https://doi.org/10.1038/s41570-020-00221-w>
- Cuello S, Abad-Álvarez I, Bartczak D, Del Castillo Busto M, Ramsay D, Pellegrino F, GoenagaInfante H (2020) The accurate determination of number concentration of inorganic nanoparticles using sPLCP-MS with the dynamic mass flow approach. *J Anal Atomic Spectro*. <https://doi.org/10.1039/C9JA00415G>
- Das D, Saikia BJ (2023) Synthesis, characterization and biological applications of cobalt oxide (Co_3O_4) nanoparticles. *Chem Phys Impact* 6:100137. <https://doi.org/10.1016/j.chphi.2022.100137>
- Durán N, Durán M, de Jesus MB, Seabra AB, Fávoro WJ, Nakazato G (2016) Silver nanoparticles: a new view on mechanistic aspects on antimicrobial activity. *Nanomed Nanotechnol Bio Med* 12(3):789–799. <https://doi.org/10.1016/j.nano.2015.11.016>
- Eid MM (2022) Characterization of nanoparticles by FTIR and FTIR-microscopy. *Consumer Nanoproducts*. https://doi.org/10.1007/978-981-16-8698-6_89
- Ertugrul MS, Nadaroglu H, Nalci OB, Hacimuftuoglu A, Alayli A (2020) Preparation of CoS nanoparticles-cisplatin bioconjugates and investigation of their effects on SH-SY5Y neuroblastoma cell line. *Cytotechnology* 72(6):885–896. <https://doi.org/10.1007/s10616-020-00432-5>
- Faisal M, Saquib Q, Alatar AA, Al-Khedhairi AA, Ahmed M, Ansari SM, Alwathnani HA, Dwivedi S, Musarrat J, Praveen S (2016) Cobalt oxide nanoparticles aggravate DNA damage and cell death in eggplant via mitochondrial swelling and no signaling pathway. *Biol Res* 49:20. <https://doi.org/10.1186/s40659-016-0080-9>
- Farhadi S, Safabakhsh J, Zaringhadam P (2013) Synthesis, characterization, and investigation of optical and magnetic properties of cobalt oxide (Co_3O_4) nanoparticles. *Nanostruct Chem*. <https://doi.org/10.1186/2193-8865-3-69>
- Ghadi FE, Ghara AR, Naeimi A (2018) Phytochemical fabrication, characterization, and antioxidant application of copper and cobalt oxides nanoparticles using *Sesbania sesban* plant. *Chem Pap* 72(11):2859–2869. <https://doi.org/10.1007/s11696-018-0506-7>
- Gheidari D, Mehrdad M, Maleki S, Hosseini S (2020) Synthesis and potent antimicrobial activity of CoFe_2O_4 nanoparticles under visible light. *Heliyon* 6(10):e05058–e05058. <https://doi.org/10.1016/j.heliyon.2020.e05058>
- Godymchuk A, Ilyashenko A, Konyukhov Y, Offor PO, Baisalova G (2022) Agglomeration and dissolution of iron oxide nanoparticles in simplest biological media. *AIMS Mater Sci* 9(4):642–652. <https://doi.org/10.3934/matersci.2022039>
- Golnarahgi Ghomi AR, Mohammadi-Khanaposhti M, Vahidi H, Kobarfard F, Ameri Shah Reza M, Barabadi H (2019) Fungus-mediated extracellular biosynthesis and characterization of zirconium nanoparticles using standard penicillium species and their preliminary bactericidal potential: a novel biological approach to nanoparticle synthesis. *Iranian J Pharm Res*. <https://doi.org/10.22037/ijpr.2019.112382.13722>
- Gong JE, Jin YJ, Kim JE, Choi YJ, Lee SJ, Kim KS, Jung YS, Cho JY, Lim Y, Kang HG, Hwang DY (2021) Comparison of cisplatin-induced anti-tumor response in CT26 syngeneic tumors of three BALB/c substrains. *Laborat Animal Res* 37(1):33. <https://doi.org/10.1186/s42826-021-00110-3>
- Goswami M, Sarma HD, Saikia M (2020) Recent developments in synthesis of cobalt oxide nanoparticles: a review. *Mol Liquids*. <https://doi.org/10.1016/j.molliq.2020.113371>
- Govindasamy R, Raja V, Singh S, Govindarasu M, Sabura S, Rekha K, Rajeswari VD, Alharthi SS, Vaiyapuri M, Sudarmani R, Jesurani S, Venkidasamy B, Thiruvengadam M (2022) Green synthesis and characterization of cobalt oxide nanoparticles using *psidium guajava* leaves extracts and their photocatalytic and biological activities. *Molecules* 27(17):5646. <https://doi.org/10.3390/molecules27175646>
- Gupta V, Kant V, Sharma AK, Sharma M (2020) Comparative assessment of antibacterial efficacy for cobalt nanoparticles, bulk cobalt and standard antibiotics: a concentration dependent study. *Nanosyst Phys Chem Mathe* 11(1):78–85. <https://doi.org/10.17586/2220-8054-2020-11-1-78-85>
- Hafeez M, Shaheen R, Akram B, Zain-ul-Abdin J, Haq S, Mahsud S, Ali S, Khan RT (2020) Green synthesis of cobalt oxide nanoparticles for potential biological applications. *Mater Res Express* 7(2):25019. <https://doi.org/10.1088/2053-1591/ab70dd>
- He Y, Gan X, Zhang L, Liu B, Zhu Z, Li T, Zhu J, Chen J, Yu H (2018) CoCl_2 induces apoptosis via a ROS-dependent pathway and Drp1-mediated mitochondria fission in periodontal ligament stem cells. *Physiol Cell Physiol* 315(3):C389–C397. <https://doi.org/10.1152/ajpcell.00248.2017>
- Hosseini-Giv N, Bahrami AR, Matin MM (2021) Application of bacterial directed enzyme prodrug therapy as a targeted chemotherapy approach in a mouse model of breast cancer. *Int J Pharm* 606:120931. <https://doi.org/10.1016/j.jipharm.2021.120931>

- Hou H, Mahdavi B, Paydarfard S, Zangeneh MM, Zangeneh A, Sadeghian N, Taslimi P, Erduran V, Sen F (2020) Novel green synthesis and antioxidant, cytotoxicity, antimicrobial, antidiabetic, anticholinergics, and wound healing properties of cobalt nanoparticles containing *Ziziphora clinopodioides* Lam leaves extract. *Sci Rep* 10(1):12195. <https://doi.org/10.1038/s41598-020-68951-x>
- Hu B, Liu R, Liu Q, Lin Z, Shi Y, Li J, Wang L, Li L, Xiao X, Wu Y (2022) Engineering surface patterns on nanoparticles: new insights into nano-bio interactions. *J Mater Chem B* 10(14):2357–2383. <https://doi.org/10.1039/d1tb02549j>
- Huang H, Wang J, Zhang J, Cai J, Pi J, Xu J-F (2021) Inspirations of cobalt oxide nanoparticle based anticancer therapeutics. *Pharmaceutics* 13(10):1599. <https://doi.org/10.3390/pharmaceutics13101599>
- Iqbal J, Numan A, Omaish Ansari M, Jafer R, Jagadish PR, Bashir S, Hasan PMZ, Bilgrami AL, Mohamad S, Ramesh K, Ramesh S (2020) Cobalt oxide nanograins and silver nanoparticles decorated fibrous polyaniline nanocomposite as battery-type electrode for high performance supercapattery. *Polymers* 12(12):2816. <https://doi.org/10.3390/polym12122816>
- Iranpour S, Bahrami AR, Nekooei S, Sh Saljooghi A, Matin MM (2021) Improving anti-cancer drug delivery performance of magnetic mesoporous silica nanocarriers for more efficient colorectal cancer therapy. *J Nanobiotechnology* 19(1):314.
- Iravani S, Varma RS (2020) Sustainable synthesis of cobalt and cobalt oxide nanoparticles and their catalytic and biomedical applications. *Green Chem* 22(9):2643–2661. <https://doi.org/10.1039/d0gc00885k>
- Jang E, Shim H-W, Ryu BH, An DR, Yoo WK, Kim KK, Kim D-W, Kim TD (2015) Preparation of cobalt nanoparticles from polymorphic bacterial templates: a novel platform for biocatalysts. *Bio Macromol* 81:747–753. <https://doi.org/10.1016/j.jbiomac.2015.09.009>
- Jiao M, Zhang P, Meng J, Li Y, Liu C, Luo X, Gao M (2018) Recent advancements in biocompatible inorganic nanoparticles towards biomedical applications. *Biomater Sci* 6(4):726–745. <https://doi.org/10.1039/c7bm01020f>
- Joudeh N, Linke D (2022) Nanoparticle classification, physicochemical properties, characterization, and applications: a comprehensive review for biologists. *J Nanobiotechnol*. <https://doi.org/10.1186/s12951-022-01477-8>
- Kalam A, Al-Sehemi AG, Al-Shihri AS, Du G, Ahmad T (2012) Synthesis and characterization of NiO nanoparticles by thermal decomposition of nickel linoleate and their optical properties. *Mater Charact* 68:77–81. <https://doi.org/10.1016/j.matchar.2012.03.011>
- Kamil Mohammad Al-Mosawi A, Bahrami AR, Nekooei S, Saljooghi AS and Matin MM (2023) Using magnetic mesoporous silica nanoparticles armed with EpCAM aptamer as an efficient platform for specific delivery of 5-fluorouracil to colorectal cancer cells. *Front Bioeng Biotechnol* 10:1095837. <https://doi.org/10.3389/fbioe.2022.1095837>
- Kavaz D, Umar H, Shehu S (2018) Synthesis, characterization, antimicrobial and antimetastatic activity of silver nanoparticles synthesized from *Ficus ingens* leaf. *Artific Cells Nanomed Biotechnol* 46(3):1193–1203. <https://doi.org/10.1080/21691401.2018.1536060>
- Kavaz D, Umar H, Zimuto T (2019) Biosynthesis of gold nanoparticles using *Scytosiphon lomentaria* (brown algae) and *Spyridia filamentosa* (red algae) from kyrenia region and evaluation of their antimicrobial and antioxidant activity. *Hacetepce J Bio Chem* 47(4):367–382. <https://doi.org/10.15671/hjbc.518593>
- Kavaz D, Abubakar AL, Rizaner N, Umar H (2021) Biosynthesized ZnO nanoparticles using *Albizia Lebbeck* extract induced biochemical and morphological alterations in wistar rats. *Molecules* 26(13):3864. <https://doi.org/10.3390/molecules26133864>
- Kavitha T, Haider S, Kamal T, Ul-Islam M (2017) Thermal decomposition of metal complex precursor as route to the synthesis of Co₃O₄ nanoparticles: antibacterial activity and mechanism. *J Alloy Compd* 704:296–302. <https://doi.org/10.1016/j.jallcom.2017.01.306>
- Khalil AT, Ovais M, Ullah I, Ali M, Shinwari ZK, Maaza M (2020) Physical properties, biological applications and biocompatibility studies on biosynthesized single phase cobalt oxide (Co₃O₄) nanoparticles via *Sageretia thea* (Osbeck). *Chemistry* 13(1):606–619. <https://doi.org/10.1016/j.arabjcs.2017.07.004>
- Khan S, Ansari AA, Khan AA, Ahmad R, Al-Obaid O, Al-Kattan W (2015) In vitro evaluation of anticancer and antibacterial activities of cobalt oxide nanoparticles. *Bio Inorganic Chem* 20(8):1319–1326. <https://doi.org/10.1007/s00775-015-1310-2>
- Kumar U, Shete A, Harle AS, Kasyutich O, Schwarzacher W, Pundle A, Poddar P (2008) Extracellular bacterial synthesis of protein-functionalized ferromagnetic Co₃O₄ nanocrystals and imaging of self-organization of bacterial cells under stress after exposure to metal ions. *Chem Mater* 20(4):1484–1491. <https://doi.org/10.1021/cm702727x>
- Lombardo D, Kiselev MA, Caccamo MT (2019) Smart nanoparticles for drug delivery application: development of versatile nanocarrier platforms in biotechnology and nanomedicine. *Nanomaterials*. <https://doi.org/10.1155/2019/3702518>
- Mehrafza, M., Tadhu, S., Khajeh, K., & Akhwan Sepahi, A. (2022). Investigating the antibacterial effect of cobalt oxide biological nanoparticles. In: abstracts of the 5th international conference on global studies in science, technology and engineering, Society for the development of new sciences and technologies, Tehran, Iran, January 25, 2022
- Mishra V, Kesharwani P, Mohd Amin MCI, Iyer AK (2017) In nanotechnology-based approaches for targeting and delivery of drugs and genes. Elsevier. <https://doi.org/10.1016/b978-0-12-809717-5.00022-1>
- Moradpoor H, Safaei M, Rezaei F, Golshah A, Jamshidy L, Hatam R, Abdullah RS (2019) Optimization of cobalt oxide nanoparticles synthesis as bactericidal agents. *Med Sci* 7(17):2757–2762. <https://doi.org/10.3889/oamjms.2019.747>
- Nakhaeepour Z, Mashreghi M, Matin MM, NakhaeiPour A, Housaindokht MR (2019) Multifunctional CuO nanoparticles with cytotoxic effects on KYSE30 esophageal cancer cells, antimicrobial and heavy metal sensing activities. *Life Sci*. <https://doi.org/10.1016/j.lfs.2019.116758>
- Naumann D, Helm D, Labischinski H (1991) Microbiological characterizations by FTIR spectroscopy. *Nature* 351(6321):81–82. <https://doi.org/10.1038/351081a0>
- Owyang SY, Zhang M, Walkup GA, Chen GE, Grasberger H, El-Zaatari M, Kao JY (2017) The effect of CT26 tumor-derived TGF-β on the balance of tumor growth and immunity. *Immunol Lett* 191:47–54. <https://doi.org/10.1016/j.imlet.2017.08.024>
- Rees P, Wills JW, Brown MR, Barnes CM, Summers HD (2019) The origin of heterogeneous nanoparticle uptake by cells. *Nat Commun*. <https://doi.org/10.1038/s41467-019-10112-4>
- Riddin TL, Gericke M, Whiteley CG (2006) Analysis of the inter- and extracellular formation of platinum nanoparticles by *Fusarium oxysporum* f. sp. lycopersici using response surface methodology. *Nanotechnology* 17(14):3482–3489. <https://doi.org/10.1088/0957-4484/17/14/021>

- Rousta A, Dorrnanian D, Elahi M (2019) Electrophoretic deposition of cobalt oxide nanoparticles on aluminum substrate. *Surf Eng* 36(9):919–928. <https://doi.org/10.1080/02670844.2019.1689899>
- Samadian H, Salami MS, Jaymand M, Azarnezhad A, Najafi M, Barabadi H, Ahmadi A (2020) Genotoxicity assessment of carbon-based nanomaterials; have their unique physicochemical properties made them double-edged swords? *Mutat Res Rev Mutat Res* 783:108296. <https://doi.org/10.1016/j.mrrev.2020.108296>
- Sanità G, Carrese B, Lamberti A (2020) Nanoparticle surface functionalization: how to improve biocompatibility and cellular internalization. *Front Mol Biosci*. <https://doi.org/10.3389/fmolb.2020.587012>
- Saravanan M, Barabadi H, Vahidi H, Webster TJ, Medina-Cruz D, Mostafavi E, Vernet-Crua A, Cholula-Diaz JL, Periakaruppan P (2020) Emerging theranostic silver and gold nanobiomaterials for breast cancer: present status and future prospects. *Handbook Nanobiomater Therapeut Diagnost Appl*. <https://doi.org/10.1016/B978-0-12-821013-0.00004-0>
- Saravanan M, Barabadi H, Vahidi H (2021) Green nanotechnology: isolation of bioactive molecules and modified approach of biosynthesis. *Biogenic Nanopart Cancer Theranost*. <https://doi.org/10.1016/B978-0-12-821467-1.00005-7>
- Sato Y, Fu Y, Liu H, Lee MY, Shaw MH (2021) Tumor-immune profiling of CT26 and Colon 26 syngeneic mouse models reveals mechanism of anti-PD-1 response. *BMC Cancer*. <https://doi.org/10.1186/s12885-021-08974-3>
- Scimeca M, Bischetti S, Lamsira HK, Bonfiglio R, Bonanno E (2018) Energy dispersive x-ray (edx) microanalysis: a powerful tool in biomedical research and diagnosis. *Histochem EJH* 62(1):2841. <https://doi.org/10.4081/ejh.2018.2841>
- SFhete RC, Fernandes PR, Borhade BR, Pawar AA, Sonawane MC, Wardue NS (2022) Review of cobalt oxide nanoparticles: green synthesis, biomedical application, and toxicity studies. *J Chem Rev*. 4(4):331–345. <https://doi.org/10.22234/jcr.2022.34398.1172>
- Stanjek H, Häusler W (2004) Basics of X-ray diffraction. *Hyperfine Interact* 154(1–4): 107–119. <https://doi.org/10.1023/B:HYPE.0000032028.60546.38>
- Taléns-Visconti R, Díez-Sales O, de Julián-Ortiz JV, Náchter A (2022) Nanoliposomes in cancer therapy: marketed products and current clinical trials. *Mol Sci* 23(8):4249. <https://doi.org/10.3390/jms23084249>
- Tripathi VK, Subramaniyan SA, Hwang I (2019) Molecular and cellular response of co-cultured cells toward cobalt chloride (CoCl₂)-induced Hypoxia. *ACS Omega* 4(25):20882–20893. <https://doi.org/10.1021/acsomega.9b01474>
- Umar H, Aliyu MR, Usman AG, Ghali UM, Abba SI, Ozsahin DU (2023a) Prediction of cell migration potential on human breast cancer cells treated with *Albizia lebbbeck* ethanolic extract using extreme machine learning. *Sci Rep* 13(1):1–16. <https://doi.org/10.1038/s41598-023-49363-z>
- Umar H, Rizaner N, Usman AG, Aliyu MR, Adun H, Ghali UM, Uzun Ozsahin D, Abba SI (2023b) Prediction of cell migration in mda-mb 231 and mcf-7 human breast cancer cells treated with *Albizia Lebbbeck* Methanolic extract using multilinear regression and artificial intelligence-based models. *Pharmaceuticals* 16(6):858. <https://doi.org/10.3390/ph16060858>
- Vahidi H, Kobarfard F, Alizadeh A, Saravanan M, Barabadi H (2021) Green nanotechnology-based tellurium nanoparticles: Exploration of their antioxidant, antibacterial, antifungal and cytotoxic potentials against cancerous and normal cells compared to potassium tellurite. *Inorg Chem Commun* 124:108385. <https://doi.org/10.1016/j.inoche.2020.108385>
- Vijayanandan AS, Balakrishnan RM (2018) Biosynthesis of cobalt oxide nanoparticles using endophytic fungus *Aspergillus nidulans*. *Environ Manage* 218:442–450. <https://doi.org/10.1016/j.jenvman.2018.04.032>
- Wang J, Ni Q, Wang Y, Zhang Y, He H, Gao D, Liang XJ (2021) Nanoscale drug delivery systems for controllable drug behaviors by multi-stage barrier penetration. *Controlled Release* 331:282–295. <https://doi.org/10.1016/J.JCONREL.2020.08.045>
- Yang C, Jiang J, Qian F, Jiang D, Wang C, Zhang W (2010) Effect of Ba doping on magnetic and dielectric properties of nanocrystalline BiFeO₃ at room temperature. *J Alloys Compounds* 507(1):29–32. <https://doi.org/10.1016/j.jallcom.2010.07.193>
- Yang JJ, Niu CC, Guo XH (2015) Mixed culture models for predicting intestinal microbial interactions between *Escherichia coli* and *Lactobacillus* in the presence of probiotic *Bacillus subtilis*. *Beneficial Microbes* 6(6):871–877. <https://doi.org/10.3920/bm2015.0033>
- Yu C, Li L, Wang S, Xu Y, Wang L, Huang Y, Hieawy A, Liu H, Ma J (2022) Advances in nanomaterials for the diagnosis and treatment of head and neck cancers: a review. *Bioact Mater* 25:430–444. <https://doi.org/10.1016/j.bioactmat.2022.08.010>
- Zhu J, Kailasam K, Fischer A, Thomas A (2011) Supported cobalt oxide nanoparticles as catalyst for aerobic oxidation of alcohols in liquid phase. *ACS Catal* 1(4):342–347. <https://doi.org/10.1021/cs100153a>

Publisher's Note

Springer Nature remains neutral with regard to jurisdictional claims in published maps and institutional affiliations.